UNIVERSITÀ DEGLI STUDI DI PADOVA
DIPARTIMENTO DI INGEGNERIA INDUSTRIALE
Department Of Industrial Engineering

Corso di Laurea Magistrale in Ingegneria dell'Energia Elettrica

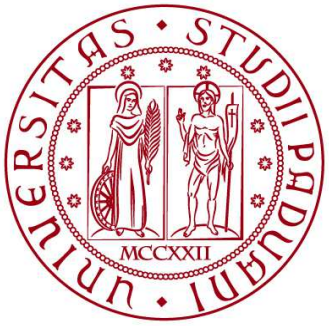

TESI DI LAUREA

Evaluation of magnetic field generated by twisted cables

Relatore:
Chiar.mo PROF. ROBERTO TURRI

Laureanda: HAILUN PENG
2028625

ANNO ACCADEMICO 2022-2023

Abstract

In this thesis the extremely low frequency magnetic field generated by twisted tripolar cables is calculated through different methods in order to compare them in terms of computational velocity and the efficiency in the evaluation of the field, with the objective to find an alternative method, simpler and faster respect to the classical Biot-Savart integration. Firstly the Biot-Savart Law is implemented on a twisted cable of finite length and its results are used as reference for all the other methods found in literature. These methods considers three infinitely long twisted helices and consists of an infinite series formulation, which contains the modified Bessel functions and their first derivatives; other simpler formulations are derived by reducing the series to the first terms. Finally a parametric equation is studied and the same heuristic method is applied directly on the Biot-Savart, which results in one new formulation, that can estimate the field values with really low errors respect to the Biot-Savart Law.

Sommario

Nella tesi sono stati implementati tutti i metodi per il calcolo del campo magnetico generato da cavi trifase elicordati, al fine di confrontarli e ricercare un metodo di buon compromesso fra l'efficienza e la velocità di calcolo.

Innanzitutto viene implementata su Matlab la classica formulazione utilizzata per i calcoli del campo magnetico, che è la Legge di Biot Savart, sia nella formulazione bidimensionale che tridimensionale. Quella bidimensionale viene implementata per la verifica della correttezza del metodo tridimensionale, allo scopo viene utilizzata come caso esempio una linea trifase interrata con posa in trifoglio (caso particolare del cavo elicordato se il passo dell'elica p tende a infinito). Una volta confermata la validità dei codici del Biot-Savart 3D, essa viene applicata nel calcolo del campo generato dal cavo tripolare elicordato, i suoi risultati sono utilizzati come riferimento per tutti gli altri metodi.

In secondo luogo, viene implementata la formulazione della serie di Hagel (che include le funzioni di Bessel modificate e le sue derivate prime) in coordinate cilindriche, i suoi risultati possono essere buoni per i casi con bassi valori del raggio di elica a e maggiori passo di elica p, ma generalmente gli errori sono elevati; inoltre, poiché va a zero molto rapidamente, per la stima della fascia di rispetto devono essere considerate cautelativamente un paio di metri addizionali.

Poiché le funzioni di Bessel sono complesse, altri metodi alternativi sono stati derivati attraverso semplificazioni di Hagel, in particolare Pettersson propone la riduzione della serie al primo termine, con ulteriori approssimazioni considerando $a << p$ e $r >> p$, ma queste formulazioni forniscono risultati con errori elevati nelle immediate vicinanze del cavo, comunque per distanze sufficientemente lontane danno risultati prossimi alla formulazione della serie completa.

Infine, viene analizzato il metodo euristico parametrico proposto da Landini basato sull'espansione in serie approssimata ai primi due termini, i risultati ottenuti sono molto buoni rispetto alla serie completa, ma questa soluzione mostra ancora errori non trascurabili rispetto ai valori di Biot-Savart.

Si decide quindi di applicare lo stesso metodo euristico di Landini direttamente sui risultati di Biot-Savart ottenendo la seguente formulazione parametrica

$$ln(B_{new}) = ln\left(2.4\pi^2 \frac{a}{p^2}\right) + ln(I) + a_0 + a_1 r + a_2 r^2 + \frac{a_3 + a_4 r}{r^{a_5}} \qquad (1)$$

questa equazione può fornire stime del campo magnetico quasi coincidente con la legge Biot-Savart nel range di distanze da 0.2m a 5m. Per distanze maggiori i risultati divergono, ma a $5m$ il campo è sicuramente molto inferiore ai limiti di qualità di $3\mu T$, anzi potrebbe essere considerato nullo.

I parametri $a_{0 \div 5}$ (eccetto a_3 che è fissato a 40) possono essere sostituiti rapidamente nell'equazione per mezzo di lookup tables in funzione dei valori di a e p; le relazioni tra i parametri e le caratteristiche geometriche dell'elica, a e p, possono essere espresse approssimativamente mediante polinomi, di grado

non superiori a 3. La formulazione risultante è più lunga di quella proposta da Landini, ma fornisce risultati migliori.

In conclusione, (1) è certamente più semplice delle formulazioni in serie, fornisce risultati migliori delle approssimazioni in serie ridotte, è più complesso dell'equazione parametrica proposta da Landini, ma i suoi risultati rispetto ai risultati di riferimento presentano errori molto più bassi di Landini, richiede un tempo computazionale sicuramente inferiore ottenendo al contempo circa le stesse stime di campo rispetto al metodo tridimensionale Biot-Savart. Si può dire che nel complesso un ottimo compromesso tra buoni risultati e velocità di calcolo.

Contents

List of Figures

List of Tables

Listings

Chapter 1

Introduction

Nowadays we are immersed in the electromagnetic fields: the electric field is generated whenever there is a difference of the electrical potential between two conductive elements, independently on the electrical devices switching on or not, and its strength increase with the voltage; the magnetic field is generated by the passage of an electric current through wires, electrical devices or cables, thus the electrical devices or the power system have to be activated, and its entity is proportional to the value of the current. The electromagnetic fields are divided into three classes according to the frequency:

- extremely low frequency field (ELF): that propagate with frequency ranging from 0 Hz up to 300 Hz, generated for example by electrical generation and distribution systems and household appliances;
- intermediate frequency field: with frequency between 300 Hz and 10 MHz, generated for example by computers;
- radio frequency field: with frequency ranging between 10 MHz and 30 GHz, propagated for example from radio, television, mobile phone antennas and microwave ovens.

The thesis deals with the magnetic field generated by the three-phase twisted cables for electric transmission application, which works at 50 Hz or 60 Hz, therefore it concerns the first group.

There are scientific researches which proves that the electromagnetic fields interact with biological tissues, its effects depends on the frequency and its entity increase by getting closer to the field source. The main effect of electromagnetic fields (especially radio frequency one) on the human body is heating, like when the microwave ovens heat food. However the levels at which we are normally exposed are much lower than the values required to produce significant warming, in addition, an Italian legislation was drawn up in 2003 imposing limits on the electromagnetic field that are lower than these threshold values,if these limits are respected, there is no scientific evidence of health risks[1].

The thesis interest only concerns the part of the limits for the protection of the population from exposure to the magnetic fields at the network frequency (50 Hz) generated by the power lines, three values are set down[2]:

1. an exposure limit equal to $100\mu T$: it must not to be exceeded in any condition of exposure of the population and precautionary measure for protection against acute effects are mandatory;

2. an attention values equal to $10\mu T$: it must not to be exceeded in residential, school and any other places used for prolonged stays higher than 4 hours/day, it is mandatory to adopt precautionary measure for protection against possible long-term effects;

3. a quality objective value equal to $3\mu T$: it is set because of the progressive mythologizing of the exposure to electromagnetic fields, it must be respected during the design of new power lines in the vicinity of children's play areas, schools, residential zones and any other places used for the stay not less than 4 hours/day, the same on the contrary, thus in the buffer zone delimited by $3\mu T$ there can be no buildings nor its pertinence such as balconies, terraces, courtyards, gardens and no parks or any equipped outdoor spaces that involve stays higher than 4 hours/day.

The twisted three-phase cables has the main characteristic of generating a lower magnetic field, because of the reduced distance between the conductors and their continuous transposition given by the twist. Due to this property they are frequently used for the electrical distribution in high, medium and low voltage, they are the most common type of the cable used for the network connection of renewable power plants, for example for connection to the transformer cabins of a wind farm or to the inverter modules for photovoltaic plant.

The widespread use makes the calculation of the ELF magnetic field in the immediate vicinity of twisted cables essential both to evaluate the magnetic impact of the power lines constructed close to the sensitive peoples or to determine the buffer zone beyond which it is respected the above mentioned quality objective limit[4]. Generally, the limit of $3\mu T$ is achieved at a very short distance from the axis of the cable, around $50 \div 80$ cm[3].

For the calculation of the magnetic induction field generated by the twisted tripolar cable, the simple two-dimensional Biot-Savart formulation based on the hypothesis of straight and parallel conductors proposed by the Italian regulation CEI 211-4 cannot be used, although it is suitable for most practical situations found for overhead and underground power lines. It is necessary to apply the Biot Savart three-dimensional integral, which require very long computational times[3].

There is in the literature a formulation in series expansions containing the modified Bessel functions and its derivatives in a reference system with cylindrical coordinates (reducible to 2 components in natural coordinates) that provides good approximate results respect to the Biot-Savart one. There are other simplified derived formulation that give nice estimations only beyond a certain

distance from the axis of the cable, anyway it is not a far distance, already at distances comparable to the helix pitch length the approximations could be considered acceptable, but the errors presented in the vicinity of the cable is really high and it is necessary to turn to the complete series formulation.

However the series formulation is more complex than the Biot-Savart one although it is faster, because of the presence of the Bessel functions and their derivatives. So further studies are made to find a parametric equation based on the first two terms of the series, it turns out an equation that always overestimate the series formulation.

The aim of the thesis is to implement and compare all the methodologies in terms of the effectiveness in the magnetic field evaluation, the simplicity of the formulation and the computational speed required by the calculation, with the final intent of seeking a method which results in a good compromise between the efficiency, the simplicity and the speed.

Chapter 2

Biot-Savart Law

2.1 General theory

The magnetic field generated by an alternating current flowing along a generic path γ is analytically described by the Biot-Savart Law:

$$\vec{B}(x_P, y_P, z_P) = \frac{\mu_0 \overline{I}}{4\pi} \int_\gamma \frac{\vec{dl} \times \widehat{u_r}}{r^2} \tag{2.1}$$

$$r = \sqrt{(x_P - x_i)^2 + (y_P - y_i)^2 + (z_P - z_i)^2}$$

where $\mu_0 = 4\pi 10^{-7}[H/m]$ is the magnetic permeability in the vacuum, $\overline{I}$ is the phasor of the circulating alternating current; along path γ are considered innumerable infinitely distanced source points $Q_i(x_i, y_i, z_i)$ and vectors $\vec{dl} = (dl_x, dl_y, dl_z)$ of infinitesimal stretches of line current tangent to them; $\vec{r} = r\widehat{u_r}$ is the vector distance between source points and observation point $P(x_P, y_P, z_P)$ with module r and direction $\widehat{u_r} = (u_{rx}, u_{ry}, u_{rz})$.

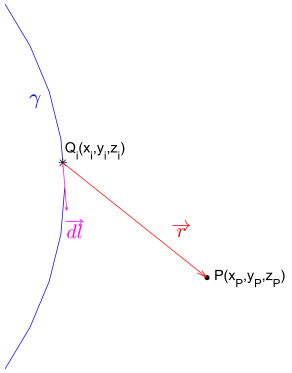

Figure 2.1: Biot-Savart Law: vectors disposition

From (2.1) are derived the following equations for phasors of spatial components of the magnetic induction field generated by a generic line current of finite length with N source points considered along it:

$$\begin{aligned}
\overline{B_x} &= \frac{\mu_0 \overline{I}}{4\pi} \sum_{i=1}^{N} \frac{dl_{yi} u_{rzi} - dl_{zi} u_{ryi}}{r_i^2} \\
\overline{B_y} &= \frac{\mu_0 \overline{I}}{4\pi} \sum_{i=1}^{N} \frac{dl_{zi} u_{rxi} - dl_{xi} u_{rzi}}{r_i^2} \\
\overline{B_z} &= \frac{\mu_0 \overline{I}}{4\pi} \sum_{i=1}^{N} \frac{dl_{xi} u_{ryi} - dl_{yi} u_{rxi}}{r_i^2}
\end{aligned} \tag{2.2}$$

therefore, the effective value of the magnetic flux density field in the observation point $P(x_P, y_P, z_P)$ is:

$$B(x_P, y_P, z_P) = \sqrt{B_x^2 + B_y^2 + B_z^2} \tag{2.3}$$

where B_x, B_y and B_z are modules of corresponding phasors[5].

These formulations could require very long computational time in case of complex current configuration, such as twisted cables or simultaneous presence of several power lines, because the expressions (2.2) have to be computed for every single current carrying conductor and the overall magnetic field is obtained by superposition of all their results; in addition, in case that a large observation area is under analysis, longer conductors with much higher number of source points are often required to be considered to get a correct estimation of the magnetic field, this causes further slowdowns of the algorithm.

However, for a line current configuration with point symmetry property and infinite length, the calculation can be simplified. Considering, for example, an infinite straight line current parallel to z-axis, the z components of the magnetic field in any observation point $P(x_P, y_P, z_P)$ generated by source points at its left side are all compensated by those at its right side, so that the overall z component of the magnetic field is null and remain only two transversal components:

$$\begin{aligned}
\overline{B_x} &= \frac{\mu_0 \overline{I}}{4\pi} \sum_{i=1}^{N} \frac{-dl_{zi} u_{ryi}}{r_i^2} \\
\overline{B_y} &= \frac{\mu_0 \overline{I}}{4\pi} \sum_{i=1}^{N} \frac{dl_{zi} u_{rxi}}{r_i^2} \\
B(x_P, y_P, z_P) &= \sqrt{B_x^2 + B_y^2}
\end{aligned} \tag{2.4}$$

Not only, the magnetic induction field generated by this infinite straight line current can be calculated by implementing the bi-dimensional formulation of the Biot-Savart Law[3]:

$$\overline{B_x} = \frac{\mu_0 \overline{I}}{2\pi} \frac{y_Q - y_P}{R^2}$$

$$\overline{B_y} = \frac{\mu_0 \overline{I}}{2\pi} \frac{x_P - x_Q}{R^2} \tag{2.5}$$
$$R = \sqrt{(x_P - x_Q)^2 + (y_P - y_Q)^2}$$

that means for any plane transversal to z-axis, only the source point $Q(x_Q, y_Q)$ at the intersection between the line and the plane have to be computed, so the effective value of the magnetic flux density field in the observation point depends only on the radial distance R, as well as the effective value of the alternating current I:

$$B(x_P, y_P, z_P) = \sqrt{B_x^2 + B_y^2} = \frac{\mu_0 I}{2\pi R} \tag{2.6}$$

In the simpler case of a power line with straight, parallel, and infinitely long conductors, the total magnetic field is obtained by superposition of all contribution from each current carrying conductor as before, but these last formulations are faster allowing to save a lot of computational time. A practical example of this case can be the underground power line, even though in the reality line current of infinite length does not exist it can still be considered as such, because electrical cables are generally long enough so that the magnetic field on the cross section at the half-length calculated by the three-dimensional method could coincides with the result obtained by the two-dimensional one, therefore the simpler bi-dimensional method is often used for a quick magnetic field evaluation.

For overhead power lines, the bi-dimensional method can still be applied, but electrical cables are arranged according to a catenary and towers or poles at two sides could be placed at different ground levels, thus the three-dimensional method is more accurate, but the bi-dimensional one can still be used for a first determination of the buffer zone widths[3].

Instead, for more complex configuration like twisted cables and multiple intersected power lines, the bi-dimensional Biot-Savart method cannot be applied. In the case of twisted cables there are other bi-dimensional formulations derived from the series expansions of the magnetic vector potential by means of the modified Bessel functions, which will be studied in the following chapters.

2.2 Comparison between Biot-Savart 3D and 2D

To compare the two Biot-Savart formulations, (2.2) and (2.5) are applied to examine a high voltage 132kV power line with three single-core cables in trefoil formation, which is a special case of twisted cables with pitch length tending to infinity. The system is symmetrical and it's carrying balanced three-phase currents with effective value equal to $I_{rms} = 1kA$; three conductors are centered at the vertices of an equilateral triangle with sides of length equal to the diameter of conductors which is set to $D = 0.1m$; the axis of the power line passing through the barycenter of conductors is taken to coinciding with the z-axis; the

encumbrance of the trefoil disposition has a radius equal to R_{line}:

$$R_{line} = \overline{AG} + \frac{D}{2} = \frac{2}{3} median + \frac{D}{2} = \frac{D}{\sqrt{3}} + \frac{D}{2} = 0.1077m \tag{2.7}$$

$$median = \frac{1}{2}\sqrt{2(\overline{AC}^2 + \overline{AB}^2) - \overline{BC}^2} = \frac{\sqrt{3}}{2} D$$

therefore the minimum radial distance from which magnetic field is evaluated is equal to $R_{min} = 0.11m$.

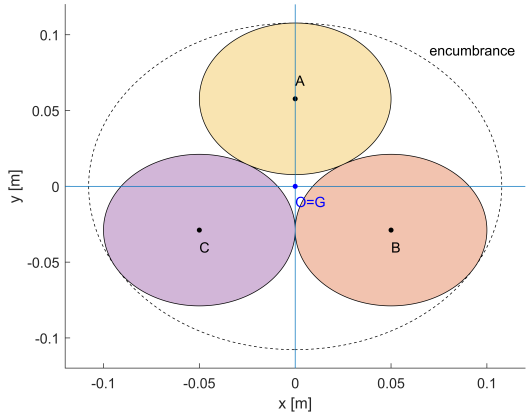

Figure 2.2: Cross-section of the trefoil formation

In order to making the comparison, the convergence of the three-dimensional method and the minimum length of conductors required by it are evaluated. Since Biot-Savart Law demonstrate that the magnetic field is inversely proportional to the square of the distance r between observation and source points, it is possible to suppose that above a certain length of conductors, source points at two extremes are too faraway and provides negligible contribution of the magnetic field to the observation point on the cross-section at the half-length, then when the three-dimensional method converge, its results should be infinitely close to the theoretical values provided by the bi-dimensional method.

An iterative method is adopted: the algorithm begins with a fixed R, a specified segmentation dl and an initial length of conductors $L = 2dl$; then $2dl$ are added to L at every iteration ($1dl$ for extreme) until the effective values of the magnetic induction field at half-length present a relative deviation minor than $10^{-4}\%$ respect to those of previous iteration, when this occurs results can be considered established and the method achieves the convergence. Theoretically source points for the three-dimensional method have to be considered at infinitesimal distances, but in order to reduce the computational time longer segmentation length is set for higher radial distance under analysis, anyway attention should be pay to maintain dl relatively small respect R. In the table 2.1 are ordered all the obtained results.

Table 2.1: Convergence of the Biot-Savart 3D method on the trefoil formation

Segmentation $dl[m]$	**Distance from the z-axis** $R[m]$	**Length of conductors** $L[m]$
0.01	0.11	7.72
	0.12	7.96
	0.13	8.2
	0.14	8.42
	0.15	8.64
	0.16	8.84
	0.17	9.04
	0.18	9.22
	0.19	9.42
	0.2	9.58
0.1	0.2	20.8
	0.31	24.2
	0.41	26.8
	0.61	30.6
	0.81	34
	0.91	35.4
	1.01	36.8
	1.11	38
	1.31	40.6
	1.51	43
	1.81	46.4
	2	48.6
1	2	102
	3.11	120
	5.11	152
	8.11	196
	11.11	240
	13.11	270
	15.11	298
	18.11	338
	20	364
10	20	640
	30.11	840
	40.11	1020
	50.11	1200
	60.11	1380
	70.11	1540
	80.11	1720
	90.11	1880
	100.11	2040

First of all, it is possible to observe that two types of segmentation are used for $R = 0.2m$, $2m$ and $20m$, taking as example $R = 0.2m$: with $dl = 0.01m$ and $L = 9.58m$ the number of source points along one conductor is equal to 959, but with $dl = 0.1m$ and $L = 20.8m$ there are only 209 source points, less than a quarter from before, therefore a longer segmentation works faster although it requires longer conductors for the convergence, because the algorithm have to compute much minor amount of source points . However, as said previously, attention should be pay to not consider an excessively long segmentation, because the method returns wrong and underestimated results due to the lose of important contributions from the nearest local source points even if it converges, tests proves that R have to be at least twice dl.

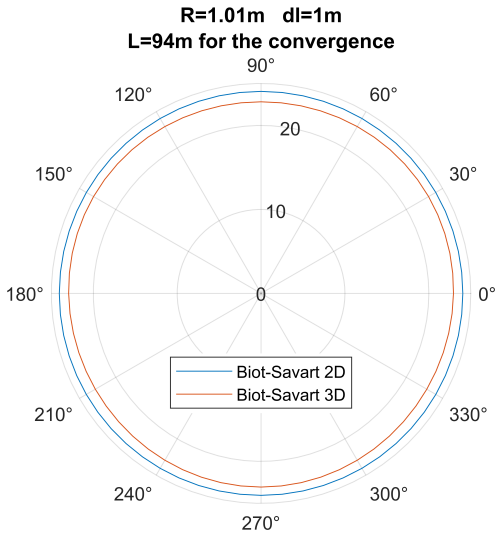

Figure 2.3: Example of a bad choice of dl:
the mean value of the magnetic field around the power line obtained with the Biot-Savart 2D method is equal to $B^{2D}_{mean} = 24.0515\mu T$, while from the Biot-Savart 3D result $B^{3D}_{mean} = 22.9377\mu T$, with a relative error equal to $e = (B^{2D}_{mean} - B^{3D}_{mean})/B^{2D}_{mean} = 4.6307\%$

In the second place, from results of L it is possible to notice that for different segmentations, to a fixed increase of the radial distance corresponds a more or less regular rise of L, therefore with a set segmentation, the length of conductors required to get a correct estimation of the magnetic field at a certain radial distance is predictable and, as clearly shown by the figure 2.5, it initially increase exponentially with exponent minor than 1 then linearly, the exponent of the first part can be more or less near to 1 and the slope of the second part more or less marked depending on the case.

A linear approximation that better fit the second part of the obtained data sets is considered for all the cases, this choice is made principally because this is the most simply and direct way to make a initial prediction of the length of conductors necessary for the analysis; furthermore coefficients are taken cautiously

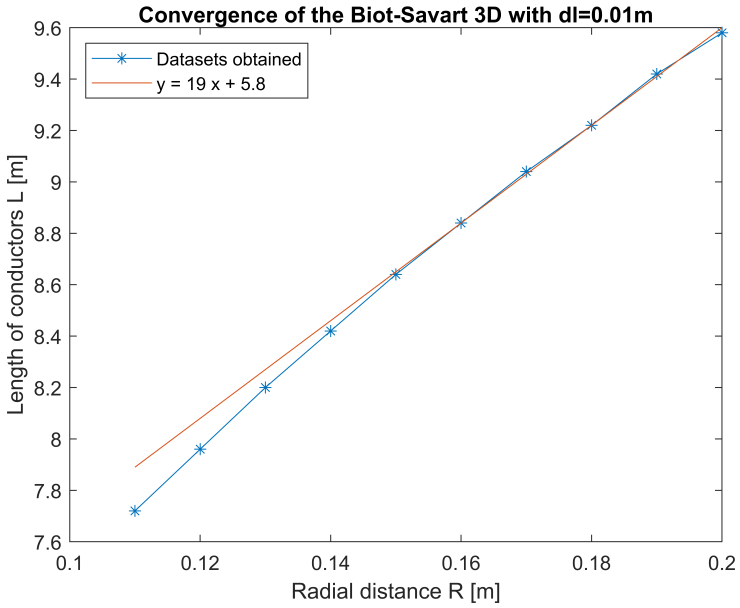

Figure 2.4: L as a function of R: case $dl = 0.01m$

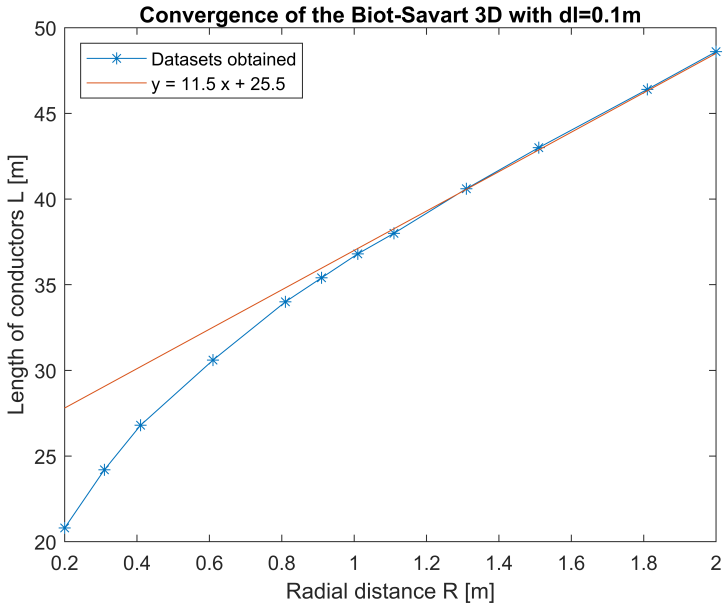

Figure 2.5: L as a function of R: case $dl = 0.1m$

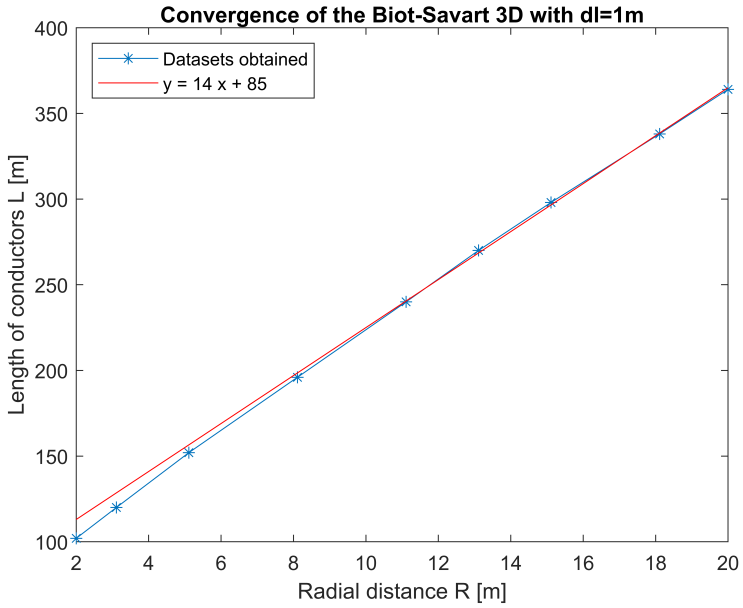

Figure 2.6: L as a function of R: case $dl = 1m$

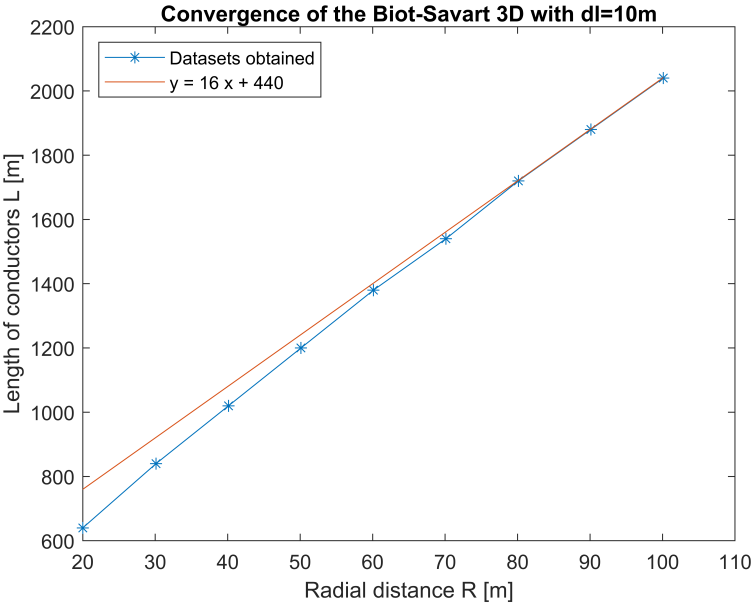

Figure 2.7: L as a function of R: case $dl = 10m$

so that L is mainly overestimated and the correct evaluation of the magnetic field is guaranteed:

$$L_{0.01m} = 19R + 5.8 \tag{2.8}$$

$$L_{0.1m} = 11.5R + 25.5 \tag{2.9}$$

$$L_{1m} = 14R + 85 \tag{2.10}$$

$$L_{10m} = 16R + 440 \tag{2.11}$$

In the reality, by testing the considered segmentation at greater distances respect to the tabulated data, it result that for cases with $dl = 0.1m$, $1m$ and $10m$ the approximated lengths L_{dl} are always overestimating the effective necessary length L in not excessive way and without burden on the calculation process, so (2.9)-(2.11) could still be considered valid; instead for $dl = 0.01m$ the calculation range $0.11-0.2m$ results included in the first exponential part, then (2.8) provide a high overestimation for the increasing of R, in this case (2.8) could be correct until $0.3m$ and over that distances a new approximation should be used:

$$L^{'}_{0.01m} = 8.5R + 9.2 \tag{2.12}$$

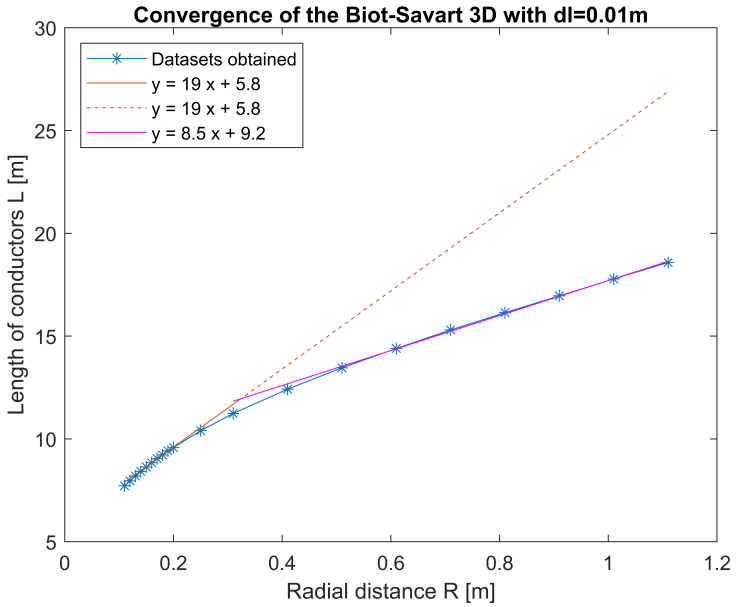

Figure 2.8: L as a function of R: case $dl = 0.01m$

Finally, the results obtained by the three-dimensional method at its convergence are effectively coincident with those from the bi-dimensional one, indeed the maximum punctual relative error presented by the first respect to the last among all performed simulations is equal to 0.1876%, so the differences can be considered negligible. In the figure 2.9 it can be see that magnetic field as a function of radial distances at different heights obtained by two methods are overlapping, while figures 2.10 and 2.11 show identical equifield lines of the magnetic induction field in a cross-section area of $16 \times 16m^2$; since the radial distances under analysis range from $R_{min} = 0.11m$ to $16\sqrt{2} \approx 23m$, segmentation $dl = 0.01m$ and length of conductors $L = 204.7m$ obtained from (2.12) are considered for the three-dimensional method, the maximum punctual relative error get from the calculation is equal to 0.0611%, therefore results could be considered coincident.

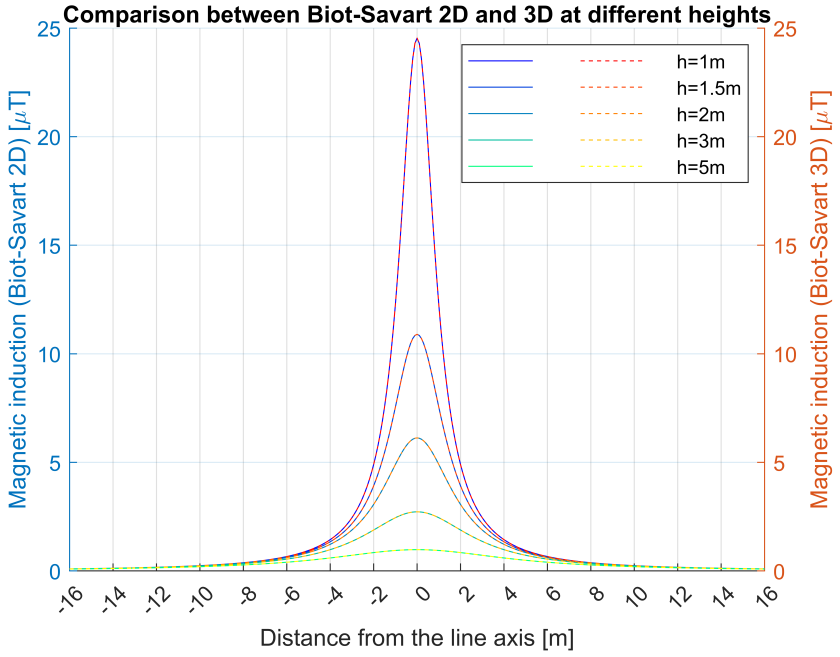

Figure 2.9: Results of Biot-Savart 3D and 2D at different heights

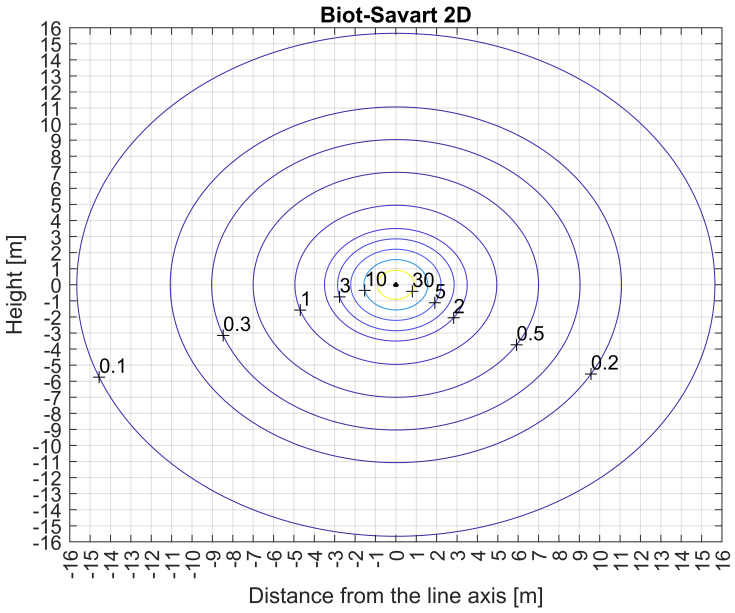

Figure 2.10: Biot-Savart 2D: equifield lines

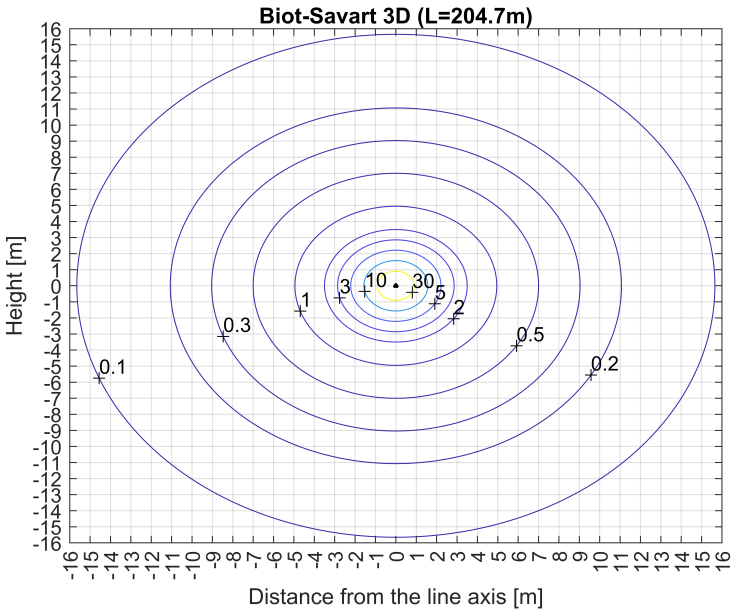

Figure 2.11: Biot-Savart 3D: equifield lines

2.3 Twisted Tripolar Cables

Once demonstrated the validity of the Biot-Savart 3D programming code and shown the correctness of its results, now it can be applied to evaluate the magnetic field generated by a twisted tripolar cable carrying balanced three-phase current with $I_{rms} = 200A$. In this configuration the three conductors parallel to z-axis are twisted together into three parallel helices centered on the z-axis and shifted by $2\pi/3$ each other, the parametrisation in Cartesian coordinates of the three helices are as follows:

$$\begin{aligned} x(t) &= a\cos(t + i\frac{2\pi}{3}) \\ y(t) &= a\sin(t + i\frac{2\pi}{3}) \\ z(t) &= pt \end{aligned} \tag{2.13}$$

with $i = 0$, 1 or 2 respectively for phase conductor a, b or c.

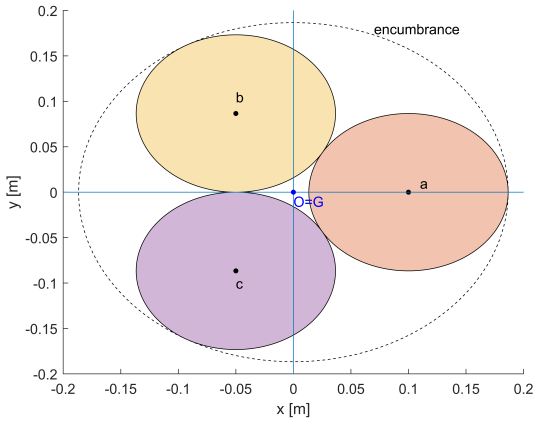

Figure 2.12: Cross-section of the twisted tripolar cable with $a = 0.1m$

The cross-section is analogous to the trefoil formation, but with conductors that continuously rotate around the barycenter moving along the z-axis; the distance between the axes of the conductors and the barycenter coincides with the radius of helices a, so a depends on the diameter of conductors, but here are considered simply 10 values of a from $0.01m$ to $0.1m$ with step of $0.01m$; after having covered a certain distance p, called the pitch length of the helix, all the conductors complete a round of 2π and return to the initial position, 13 values of p from $0.8m$ to $2m$ with step of $0.1m$ are take in consideration[4].

The diameter of conductors D and the radius of their encumbrance R_{line} are calculated backwards from values of the helices radius a by using (2.7):

$$D = \frac{2}{\sqrt{3}} median = \frac{2}{\sqrt{3}}\frac{3}{2}a = \sqrt{3}a \tag{2.14}$$

$$R_{line} = a + \frac{D}{2} = \left(1 + \frac{\sqrt{3}}{2}\right) a$$

from results it have been decided that the minimum radial distance $Rmin$ from which magnetic field is evaluated is equal to $0.1m$ for $a = 0.01 \div 0.05m$ and equal to $0.2m$ for $a = 0.06 \div 0.1m$.

Table 2.2: D, R_{line} and R_{min} as a function of the considering a

$a[m]$	$D[m]$	$R_{line}[m]$	$R_{min}[m]$
0.01	0.0173	0.0187	0.1
0.02	0.0346	0.0373	0.1
0.03	0.0520	0.0560	0.1
0.04	0.0693	0.0746	0.1
0.05	0.0866	0.0933	0.1
0.06	0.1039	0.1120	0.2
0.07	0.1212	0.1306	0.2
0.08	0.1386	0.1493	0.2
0.09	0.1559	0.1679	0.2
0.10	0.1732	0.1866	0.2

As previously done with trefoil formation, the convergence have to be analyzed before going to study the results, because there is a risk of having incorrect magnetic field values if a short cable is considered. The same iterative method as before is adopted: the parameter t is taken at distances of $\pi/100$ between $-T = -2k\pi$ and $T = 2k\pi$, with k a natural number; then 2π are added to each side at every iteration until the effective values of the magnetic field on the cross section at $t = 0$ ($z = 0$) present a relative deviation minor than $10^{-3}\%$ respect to those of previous iteration. The radial distance in which the magnetic field are evaluated is set to $5m$, sufficiently far away that the field can be considered to be zero or almost zero within it, therefore later the observation distances will cover ranges between R_{min} and $5m$, but it cannot exceed $5m$.

In the table 2.3 are ordered the convergence length of the considered twisted cable configurations: it can be observed that the helix radius do not effect on the convergence; instead the cable length increases when the pitch length decreases, that because the shorter is the p the more complex (twisted) is the configuration, so the required cable length for the convergence is greater, while for increasing p the configuration become more and more like the trefoil formation then L decrease. The maximum of the parametrisation is set to a cautionary value of $T = 300\pi$ for all the twist cables configuration in the subsequent analysis.

Firstly, the general behaviour of the magnetic field is evaluated by considering a twisted cable with fixed $a = 0.1m$ and $p = 1m$. At very close distances from the cable, the magnetic field present a sinusoidal variation with period $2\pi/3$ at different angular position: it is maximum at the axes of the conductors where it is supposed to be concentrated the current ($\theta = 0°$, $120°$ and $240°$), then it decrease moving away until it reaches the minimum at $\theta = 60°$, $180°$

Table 2.3: Convergence of the Biot-Savart 3D method on twisted tripolar cables

Helix radius $a[m]$	**Pitch length** $p[m]$	**Parameter maximum** $T = 2k\pi[m]$	**Cable length** $L[m]$
0.01	0.8	$129{\cdot}2\pi$	1296.7992
	1	$80{\cdot}2\pi$	1005.2468
	1.5	$41{\cdot}2\pi$	772.8318
	2	$29{\cdot}2\pi$	728.8495
0.05	0.8	$129{\cdot}2\pi$	1296.7992
	1	$80{\cdot}2\pi$	1005.2468
	1.5	$42{\cdot}2\pi$	791.6813
	2	$29{\cdot}2\pi$	728.8495
0.1	0.8	$128{\cdot}2\pi$	1286.7461
	1	$80{\cdot}2\pi$	1005.2468
	1.5	$42{\cdot}2\pi$	791.6813
	2	$29{\cdot}2\pi$	728.8495

and 300°, that are the furthest positions from the currents, after that it increase again by getting closer to the next conductors; the amplitude of the variations decrease with the distancing from the cable until to be almost null at around $R = 0.37m$, from here the magnetic field presents approximately constant values around the cable and could be considered uniform; however to be precise, the magnetic field is keeping to vary slightly with the same frequency, but as opposed to before it presents higher value at $\theta = 60°$ respect to $\theta = 0°$.

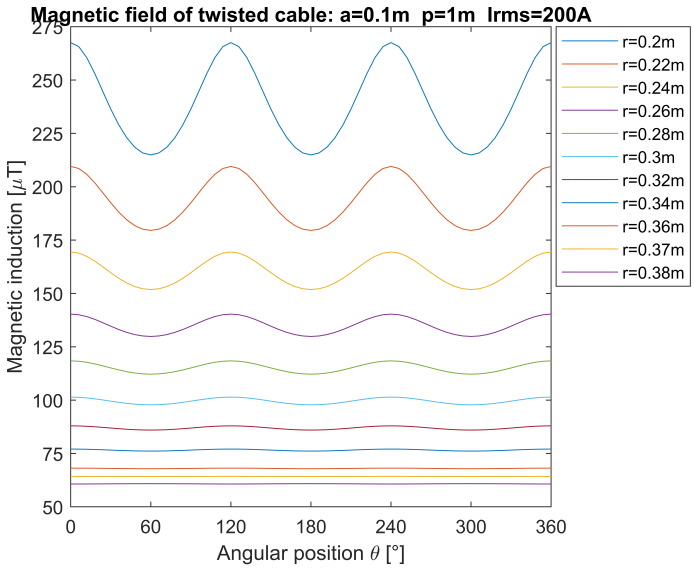

Figure 2.13: The magnetic field around a twisted cable

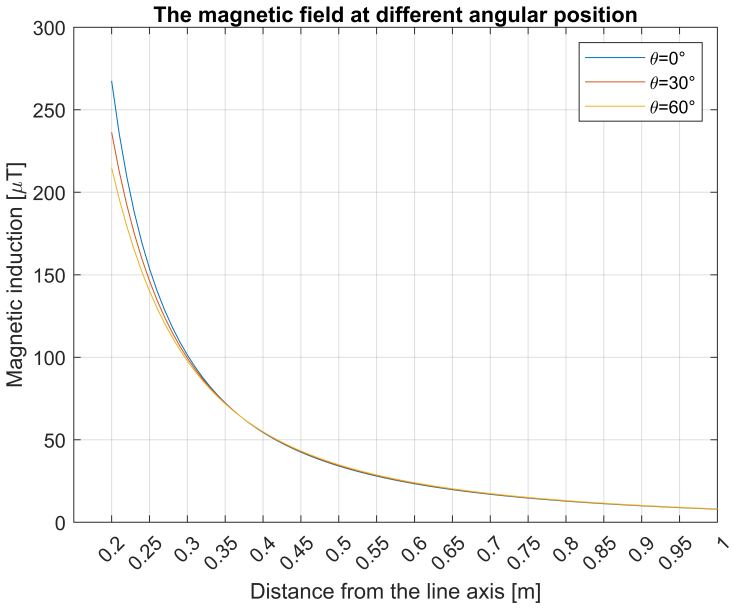

Figure 2.14: The magnetic field from $0.2m$ to $1m$ at different angular position

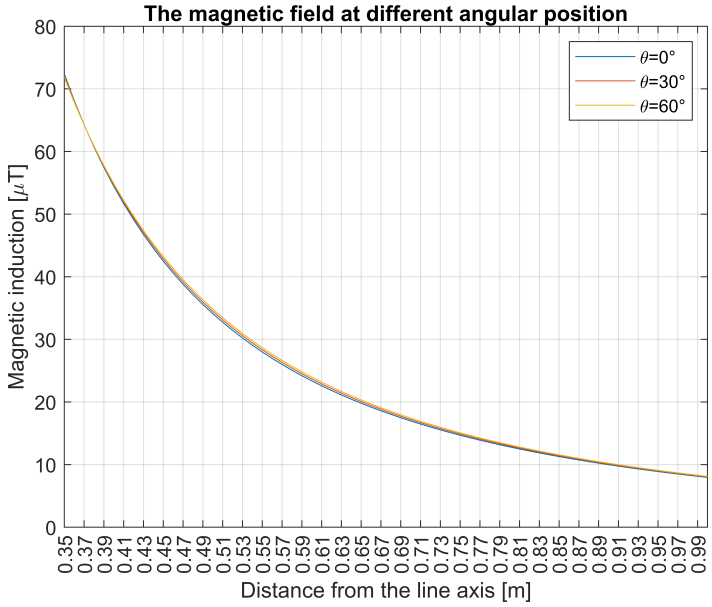

Figure 2.15: The magnetic field from $0.35m$ to $1m$ at different angular position

Since the magnetic field at higher radial distances is of more practical interest, it is more convenient and cautionary to take the magnetic field at $\theta = 60°$ as reference[4].

Secondly, the behaviour of the magnetic field at the variation of the parameters a and p are observed. By set the radius of the helices at $0.1m$ and varying the pitch length from $0.8m$ to $2m$ the magnetic field present extremely small variations: at $\theta = 60°$ it initially decrease with the rise of p, but for the radial distance after around $0.45m$, the magnetic field is higher for increasing p [figure 2.16]; instead, at $\theta = 0°$ the magnetic field is always higher with greater p, graphically it means that the curve of the magnetic induction as a function of the radial distance $B(r)$ is shifting upwards vertically for increasing p [figure 2.17]; these differences decrease with minor a. While with pitch length fixed to $2m$ and the helix radius varying from $0.01m$ to $0.1m$, the magnetic field increase proportionally with the rise of a, at both $0°$ and $60°$ [figure 2.18].

All these results perfectly reflect the theory: the magnetic field should be lowered by twisting the conductors and the level of the reduction depends on the entity of the twisting, that is the pitch length; instead the helix radius do not influence on the magnetic field, lower field intensity is presented with lower a at the same radial distance only because the cables have minor encumbrance and the magnetic field start to decrease at lower radial distances.

Finally, the results of the magnetic field generated by the twisted tripolar cable are compared respect to those of the trefoil formation with the same diameter of conductors. In the table 2.4 below are indicated for some of twisted configurations the radial distances at which the fixed percentages of reduction are reached, and at the last column the reduction percentage at distance of $5m$. As anticipated, lower pitch length has higher reduction effect, in particular this effect is accentuated with increasing helix radius and at minor radial distances; after a certain r and a reduction of around 20% the advantage of the configurations with higher a is nullified and at $5m$ those with $a = 0.01m$ have even reduction slightly higher respect to $a = 0.1m$. In the figure 2.19 are represented two cases of the comparison between trefoil and twisted configuration, one with the maximized reduction effect ($a = 0.1m$ and $p = 0.8m$) and the other one with the lowest reduction percentage ($a = 0.01m$ and $p = 2m$).

Table 2.4: The level of the field reduction at different p and a

$p[m]$	$a[m]$	1%	5%	15%	30%	50%	$5m$
2	0.01	1.16m	1.89m	2.83m	3.89m	/	46.2800%
	0.1	0.68m	1.83m	2.81m	3.88m	/	46.2766%
1.6	0.01	0.92m	1.51m	2.26m	3.11m	4.22m	62.1071%
	0.1	0.35m	1.45m	2.25m	3.11m	4.22m	62.0741%
1.2	0.01	0.69m	1.13m	1.70m	2.33m	3.17m	80.5695%
	0.1	0.20m	1.07m	1.68m	2.33m	3.17m	80.5261%
0.8	0.01	0.45m	0.75m	1.13m	1.56m	2.11m	95.8001%
	0.1	0.20m	0.69m	1.12m	1.56m	2.12m	95.7766%

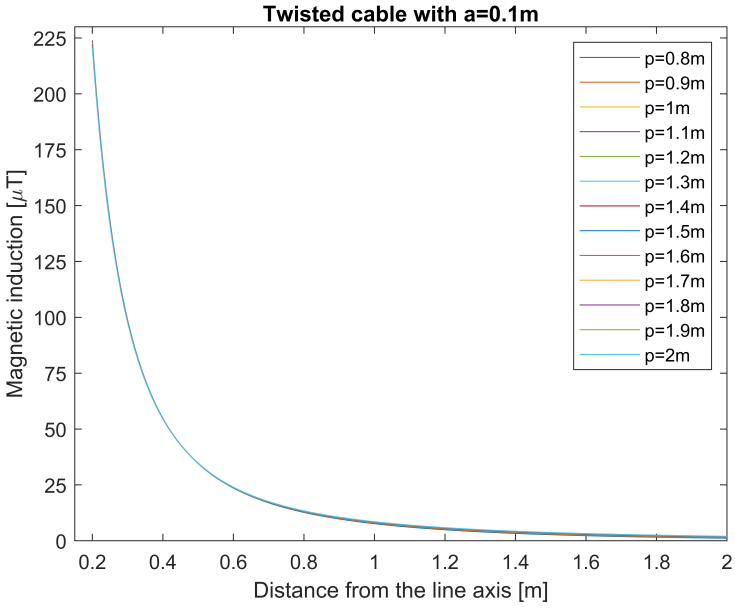

Figure 2.16: The magnetic field at $\theta = 60°$ with constant a and variable p

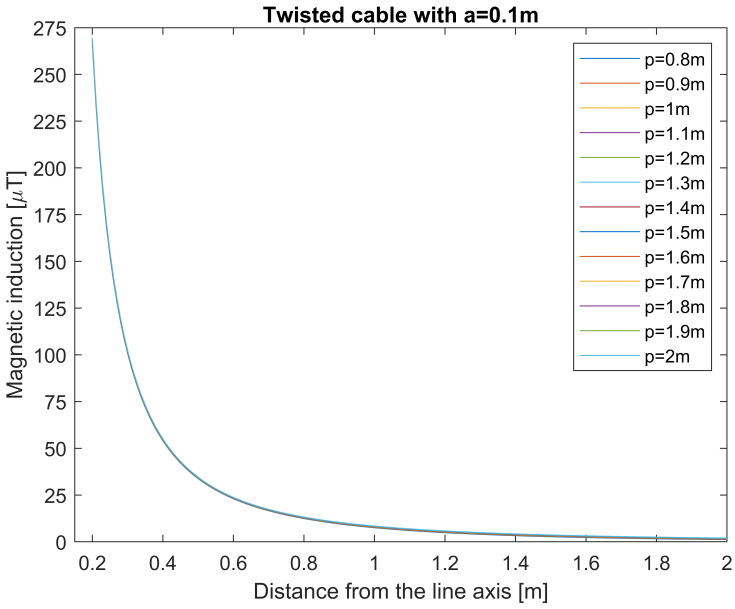

Figure 2.17: The magnetic field at $\theta = 0°$ with constant a and variable p

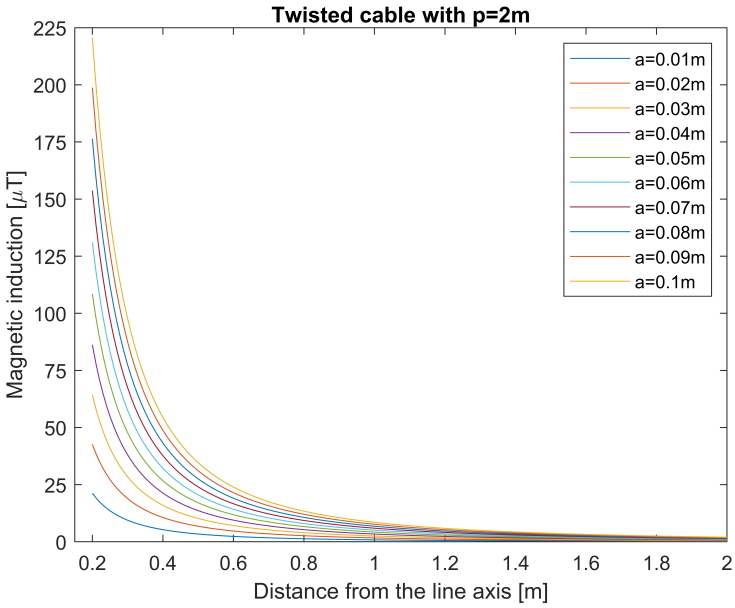

Figure 2.18: The magnetic field at $\theta = 60°$ with constant p and variable a

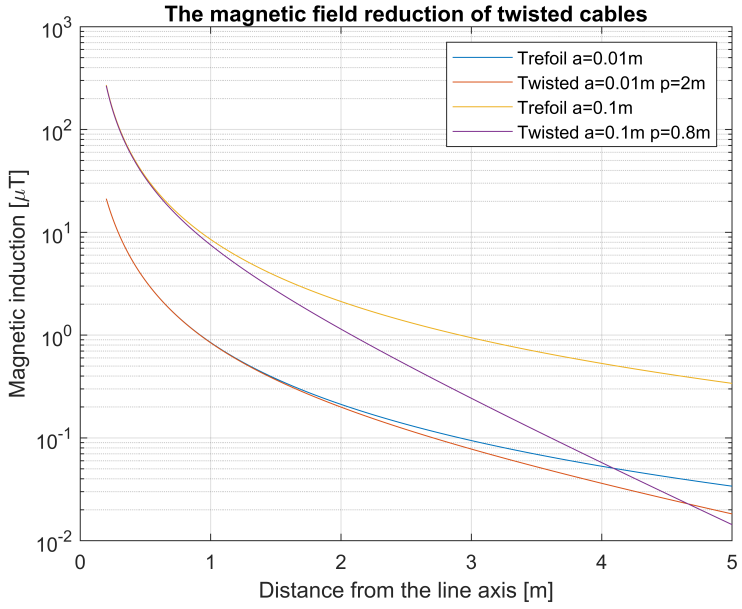

Figure 2.19: The field reduction effect of twisted cables

2.4 Matlab codes

Two important Matlab functions are adopted in this chapter: the first function is BiotSavart3D, that implements the three-dimensional Biot-Savart formulation as the name suggests, the second function is obviously BiotSavart2D, used to check the correct functioning of the previous one on the trefoil formation. The BiotSavart3D function require 6 inputs, that are:

1. a vector q indicating z-position of parameters along straight conductors or a vector t containing parameters along helices;
2. a structured matrix C where are ordered separately x, y and z coordinates of the development of each conductors in the space;
3. a variable Pz that indicate the z-position of the cross-section, it is always fixed to zero where is the middle-length of the cables;
4. two vectors Px, Py with indicated the Cartesian coordinates of observation points on the cross-section where is wanted to calculate the magnetic field; if Polar coordinates are used, they have to be converted into Cartesian coordinates before to enter them into the function:

$$P_x = r\cos\theta \quad P_y = r\sin\theta$$

5. a matrix I with the effective values of the current circulating in each conductor on the first column and the correspondent phases on the second column.

Bellow are input data for the trefoil formation and the twisted configuration:

Listing 2.1: Cables in trefoil formation

```
    %% THREE SINGLE-CORE CABLES IN TREFOIL FORMATION
D1f=0.1; % conductor diameter [m]
median=sqrt(3)/2*D1f; % [m]
R=2/3*median+D1f/2; % [m]
% observation points P have to be taken outside cables
% R is rounded up to the nearest [dm] dimenion
Rmin=ceil(R*10)/10;

dq=round(0.01,4); % segmentation of conductors [m]
L=round(204.7,4); % conductor length [m]
q=-L/2:dq:L/2; % parametrisation along conductors
l=ones(1,length(q));

% Cables disposition:
% {C} = { [x] [y] [z] }
% [x/y/z] = [phase a; phase b; phase c]
%            3(row)xlength(q)(column)
```

```
C.x=[D1f/2*l;        0*l;             -D1f/2*l];
C.y=[-median/3*l;    2/3*median*l;    -median/3*l ];
C.z=[  q;            q;                 q    ];

Irms=1000; % current effective value [A]
I=[Irms  120
   Irms  240
   Irms  360];

Px=-16:0.1:16;    Py=Px;    Pz=0;  % calculation area
% recall function
[Beff,Q,dl]=BiotSavart3D(q,C,Px,Py,Pz,I);
```

Listing 2.2: Twisted tripolar cable

```
    %% TWISTED TRIPOLAR CABLE
a=0.01; % helices radius [m]
median=3/2*a; % median=sqrt(3)/2*D1f [m]
D1f=2/sqrt(3)*median;
R=a+D1f/2;
Rmin=ceil(R*100)/100;

p=1; % pitch length [m]
dt=pi/100; % segmentation of conductors [m]
t=-300*pi:dt:300*pi; % parametrisation
l=p*t; % cable length [m]

h=0; % height of the cable respect to the ground [m]
C.x=[a*cos(t);  a*cos(t+2*pi/3);  a*cos(t-2*pi/3)];
C.y=[a*sin(t)+h;a*sin(t+2*pi/3)+h;a*sin(t-2*pi/3)+h];
C.z=[l;         l;                l];

Irms=200; % current effective value [A]
I=[Irms   0
   Irms  120
   Irms  240];

r=Rmin:0.1:3;   theta=0:pi/30:2*pi; % calculation area

Px=zeros(length(theta),length(r));
Py=zeros(length(theta),length(r));
Beff3D=zeros(length(theta),length(r));
for ir=1:length(r)
    for ia=1:length(theta)
        Px(ia,ir)=r(ir)*cos(theta(ia));
        Py(ia,ir)=r(ir)*sin(theta(ia));
    [Beff,Q,dl]=Laplace(t,C,Px(ia,ir),Py(ia,ir),0,I);
```

```
        Beff3D(ia,ir)=Beff;
    end
end
```

After received input data, the function begin its work: it calculates phasors of currents for each conductor and already multiply them by 0.1 derived from

$$\frac{\mu_0}{4\pi}10^6 = \frac{4\pi 10^{-7}}{4\pi}10^6 = 0.1$$

so that the results of magnetic field is expressed in $[\mu T]$ when I_{rms} is expressed in $[A]$; with a cycle for, it define a structured matrix dl where are saved the components of tangent vectors $\vec{dl}$ as the difference between two consecutive parameters of the matrix C, and a structured matrix Q with Cartesian coordinates of source points Q_i taken as midpoints; with three cascading cycles for, it consider one by one the observation points P calculating the distances $r = \overline{PQ_i}$ and the unit vector $\widehat{u_r}$ for all the source points (saved in a structured matrix R), then it calculate all the contribution (saved in a structured matrix dB)

$$dB(x,y,z) = \frac{\vec{dl} \times \widehat{u_r}}{r^2}$$

and finally, by summing up the product of each single contribution dB.x, dB.y and dB.z with the corresponding phasor current, the phasors of spatial components of the magnetic field in the observation points are obtained, the effective magnetic field is calculated from the square root of the sum of the squared modules of the phasors components.

The function BiotSavart3D returns three output: the three-dimensional matrix Beff containing the effective value of the magnetic field in each observation point expressed in $[\mu T]$; and the two structured matrix dl and Q, used only to verify that source points and their related tangent vector are placed properly.

The following is the Matlab script of the function BiotSavart3D:

Listing 2.3: Three-dimensional Biot-Savart method

```
    %% BIOT-SAVART 3D METHOD
function [Beff,Q,dl]=BiotSavart3D(q,C,Px,Py,Pz,I)
%            muo              Ifase
% B(x,y,z) = --- * integral ( ----  dl x Ru )
%            4*pi              r^2

    %% Data
alfa=I(:,2)*pi/180;
Ifase=I(:,1).*(cos(alfa)+1i*sin(alfa))*0.1;
% the coefficient 0.1 is given by mu*10^6/(4*pi)=0.1
% (mu= 4*pi*10^-7), thus B results in [microT]
% when I is expressed in [A]
n=length(q)-1; % number of segments along conductors
f=size(C.x,1); % number of conductors
```

```
for i=1:n
    % components of vector tangent to each
    % segment (n column) of each conductor (f row)
    dl.x(:,i)=C.x(:,i+1)-C.x(:,i);
    dl.y(:,i)=C.y(:,i+1)-C.y(:,i);
    dl.z(:,i)=C.z(:,i+1)-C.z(:,i);
    % coordinates of source point Q of each
    % segment (n column) of each conductor (f row)
    Q.x(:,i)=C.x(:,i)+dl.x(:,i)/2;
    Q.y(:,i)=C.y(:,i)+dl.y(:,i)/2;
    Q.z(:,i)=C.z(:,i)+dl.z(:,i)/2;
end

    %% Calculation
% counters
nx=length(Px);  ny=length(Py);  nz=length(Pz);
Beff=zeros(nx,ny,nz);

for ix=1:nx
% components of vector r from source point Qi to
% calculation point P(ix,iy,iz): R.x/y/z=[f x n]
R.x=Px(ix)-Q.x;
    for iy=1:ny
    R.y=Py(iy)-Q.y;
        for iz=1:nz
        R.z=Pz(iz)-Q.z;

        r=sqrt(R.x.^2+R.y.^2+R.z.^2); % distance QP

        % unit vector u_r
        R.xu=R.x./r;    R.yu=R.y./r;    R.zu=R.z./r;

        % dB=dlxR/r^2
        dB.x=(dl.y.*R.zu-dl.z.*R.yu)./r.^2;
        dB.y=(-dl.x.*R.zu+dl.z.*R.xu)./r.^2;
        dB.z=(dl.x.*R.yu-dl.y.*R.xu)./r.^2;

        % Ifase.*sum(dB.x,2)=total x-contribution of
           each single conductor [f x 1]
        % phasor Bx=sum(I.*sum(dB.x,2))=total x-
           contribution of all condustors [1 x 1]
        % Bx=abs(phasor Bx)=module
        % Beff(ix,iy,iz)=sqrt(Bx^2+By^2+Bz^2)
        Beff(ix,iy,iz)=...
            sqrt(abs(sum(Ifase.*sum(dB.x,2)))^2+ ...
                 abs(sum(Ifase.*sum(dB.y,2)))^2+ ...
```

```
                    abs(sum(Ifase.*sum(dB.z,2)))^2);
        end
    end
end
end
```

The function BiotSavart2D that implement the bi-dimensional Biot Savart formulation use the same logic although much simpler. It require only four inputs:

1. the same vectors Px, Py as before, with indicated the coordinates of observation points on the cross-section where is wanted to calculate the magnetic field;
2. the structured matrix C, from which only the x and the y coordinates of the position of conductors on the cross-section at the mid-length are extracted, for the straight lines all columns are the same, so actually any plane can be considered;
3. and the matrix I with the effective values of the circulating current on the first column and the relative phases on the second column.

This time the function calculates phasors of currents as before, but it multiplies them by 0.2 derived from

$$\frac{\mu_0}{2\pi}10^6 = \frac{4\pi 10^{-7}}{2\pi}10^6 = 0.2$$

thus the results of magnetic field is expressed with $[\mu T]$ when I_{rms} is in $[A]$. Then, with only two cascading cycles for, it calculate directly the magnetic components, Bpx and Bpy, in every observation point exercised by each source points by means of (2.5); the effective magnetic field is calculated from the square root of the sum of the squared modules of all the contributions and is saved in the two-dimensional matrix Beff, that is returned as output.

Listing 2.4: Bidimensional Biot-Savart Method

```
    %% BIOT-SAVART 2D
function Beff=BiotSavart2D(Px,Py,C,I)

    %% Data
Cx=C.x(:,1);    Cy=C.y(:,1); % source points position
alfa=I(:,2)*pi/180;
Ic=I(:,1).*(cos(alfa)+1i*sin(alfa))*0.2;
% the coefficient 0.2 is given by mu*10^6/(2*pi)=0.2
% (mu= 4*pi*10^-7) thus B results in [microT]
% when I is expressed in [A]

    %% Calculation
```

```
nx=length(Px);  ny=length(Py); % counters
Beff=zeros(nx,ny);
for ix=1:nx
 for iy=1:ny
     % Magnetic components exercised by each source
     % points in the point P(ix,iy)
    Bpx = Ic.*((Cy-Py(iy))./ ...
              ((Px(ix)-Cx).^2+(Py(iy)-Cy).^2));
    Bpy = Ic.*((Px(ix)-Cx)./ ...
              ((Px(ix)-Cx).^2+(Py(iy)-Cy).^2));
     % Bx=sum(Bpx) = comprehensive phasor component
     % abs(Bx) = the module
     % Beff=sqrt(Bx^2+By^2)
    Beff(ix,iy)=(sqrt(abs(sum(Bpx))^2 ...
                      +abs(sum(Bpy))^2));
 end
end
```

Chapter 3

The magnetic field of an infinitely long helical line current

3.1 Pioneering works

Traditionally the Biot-Savart Law is often used in the calculation of the magnetic fields of differently configured current lines, and among these also the twisted three-phase line currents, but it requires very long computational time, so there are other simpler and faster methods that can provide at the same time a good evaluation of the the magnetic field generated by twisted cables?

Let's consider an infinitely long helical line current with radius a and pitch length p, it is centered along z-axis and intersects the plane $z = 0$ at an angular position φ_0.

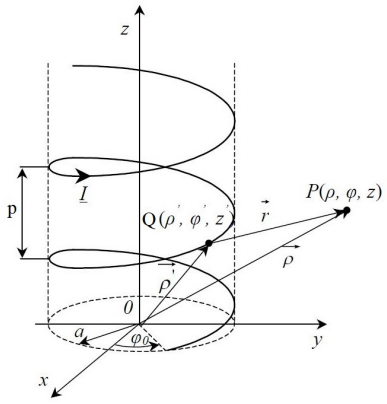

Figure 3.1: The helical line current

The magnetic field generated by this line current can be evaluated considering the magnetic vector potential:

$$\vec{B} = \nabla \times \vec{A} \tag{3.1}$$

$$\vec{A} = \frac{\mu_0 \overline{I}}{4\pi} \int_\gamma \frac{\vec{dl}}{r} \tag{3.2}$$

where $\mu_0 = 4\pi 10^{-7}[H/m]$ is the magnetic permeability in the vacuum, $\overline{I}$ is the phasor of the circulating alternating current; the vector element $\vec{dl}$ represents infinitesimal stretches of field sources on the line current, with its same direction; and r is the distance between observation point P and source point Q.

Firstly Buchholz H. derived from (3.2) the following cylindrical components of the magnetic vector potential:

$$\begin{aligned} A_\rho(\rho,\varphi,z) &= -\frac{\mu_0 \overline{I}}{4\pi} ak \int_{-\infty}^{\infty} \frac{sin(\varphi_0 - \varphi + kz^{'})}{r} dz^{'} \\ A_\varphi(\rho,\varphi,z) &= \frac{\mu_0 \overline{I}}{4\pi} ak \int_{-\infty}^{\infty} \frac{cos(\varphi_0 - \varphi + kz^{'})}{r} dz^{'} \\ A_z(\rho,\varphi,z) &= \frac{\mu_0 \overline{I}}{4\pi} \int_{-\infty}^{\infty} \frac{dz^{'}}{r} \end{aligned} \tag{3.3}$$

where $k = 2\pi/p$ is a coefficient depending on the pitch length[5].

The distance between the observation point and the variable source point on the line current can be expressed by the following series expansion:

$$\frac{1}{r} = \sum_{n=0}^{\infty} (2 - \delta_{0n}) cos(n(\varphi_0 - \varphi + kz^{'})) \int_0^{\infty} e^{-|z-z^{'}|\lambda} J_n(\rho\lambda) J_n(\rho^{'}\lambda) d\lambda \tag{3.4}$$

where J_n is the $n-$th order Bessel function of the first kind, δ_{0n} is the Kronecker symbol, and λ is the variable of the integration. Therefore, by substituting (3.4) into (3.3) and by means of some trigonometric theorems and Bessel functions' integral properties, Hagel R. rewritten the magnetic vector potential components considering the observation point in the region $\rho > a$:

$$\begin{aligned} A_\rho = -\frac{\mu_0 \overline{I}}{2\pi} ak \Big\{ & I_0(ak) K_0(\rho k) sin(\varphi_0 - \varphi + kz) + \\ & + I_1(2ak) K_1(2\rho k) sin(2(\varphi_0 - \varphi + kz)) + \\ & + \sum_{n=2}^{\infty} \Big[I_n((n+1)ak) K_n((n+1)\rho k) sin((n+1)(\varphi_0 - \varphi + kz)) + \\ & - I_n((n-1)ak) K_n((n-1)\rho k) sin((n-1)(\varphi_0 - \varphi + kz)) \Big] \Big\} \end{aligned}$$

$$
\begin{aligned}
A_\varphi = \frac{\mu_0 \overline{I}}{2\pi} ak \Bigg\{ & \frac{a}{2\rho} + I_0(ak)K_0(\rho k)sin(\varphi_0 - \varphi + kz) + \\
& + I_1(2ak)K_1(2\rho k)sin(2(\varphi_0 - \varphi + kz)) + \\
& + \sum_{n=2}^{\infty} \Bigg[I_n((n+1)ak)K_n((n+1)\rho k)cos((n+1)(\varphi_0 - \varphi + kz)) + \\
& + I_n((n-1)ak)K_n((n-1)\rho k)cos((n-1)(\varphi_0 - \varphi + kz)) \Bigg] \Bigg\}
\end{aligned} \tag{3.5}
$$

$$
A_z = \frac{\mu_0 \overline{I}}{2\pi} \left[\int_0^{\infty} \frac{J_0(a\lambda)J_0(r\lambda)}{\lambda} d\lambda + 2 \sum_{n=1}^{\infty} I_n(nak)K_n(n\rho k)cos(n(\varphi_0 - \varphi + kz)) \right]
$$

By applying the curl operation to these last formulations with the use of the recurrence relations of the modified Bessel functions, in the end Hagel R. obtained the cylindrical components of the magnetic field as infinite series:

$$
\begin{aligned}
B_\rho(\rho, \varphi, z) &= -\frac{\mu_0 \overline{I}}{\pi} ak^2 \sum_{n=1}^{\infty} n I_n^{'}(nka) K_n^{'}(nk\rho) sin(n(\varphi_0 - \varphi + kz)) \\
B_\varphi(\rho, \varphi, z) &= \frac{\mu_0 \overline{I}}{2\pi\rho} + \frac{\mu_0 \overline{I}}{\pi\rho} ak \sum_{n=1}^{\infty} n I_n^{'}(nka) K_n(nk\rho) cos(n(\varphi_0 - \varphi + kz)) \\
B_z(\rho, \varphi, z) &= -\frac{\mu_0 \overline{I}}{\pi} ak^2 \sum_{n=1}^{\infty} n I_n^{'}(nka) K_n(nk\rho) cos(n(\varphi_0 - \varphi + kz))
\end{aligned} \tag{3.6}
$$

where I_n and K_n are the modified Bessel functions of first and second kind, $I_n^{'}$ and $K_n^{'}$ their respective first derivative.

It should be pointed out that these components are valid only for the calculation range outside the helix ($\rho > a$) that is on the interests of the thesis, but Hagel derived the formulations also for observation points inside the helix ($\rho < a$) adopting the same procedure[7].

3.2 Three infinitely long twisted helices

The Hagel's formulations describes the magnetic field generated only by one conductor under helix form, it cannot be applied to the three-phase system, since the superposition of effects is not valid due to the impossibility to consider current phasors disposition on an infinite path. However the alternating currents circulating in the twisted tripolar cable can be expressed as a function of the time:

$$
I_i = \sqrt{2} I \sin(\omega t + \psi_i) = \sqrt{2} I \sin\left(\omega t + (i-1)\frac{2\pi}{3}\right) \tag{3.7}
$$

with I the effective value of the currents, ω the angular frequency and ψ_i the phase angle of the current in the i-th conductor (i = 1,2,3). The helices are considered to intersect the plane $z = 0$ at angular positions

$$
\varphi_{0i} = (i-1)\frac{2\pi}{3}
$$

By replacing (3.7) to the current phasors in (4.1), the sum of the three currents contributions can be obtained with few mathematical steps:

$$B_\rho = -\frac{\mu_0\sqrt{2}I}{\pi}ak^2\sum_{n=1}^{\infty}\sum_{i=1}^{3}nI_n^{'}(nka)K_n^{'}(nk\rho)sin(\omega t+\psi_i)sin(n(\varphi_{0i}-\varphi+kz))$$

$$\begin{aligned}B_\varphi =&\frac{\mu_0\sqrt{2}I}{2\pi\rho}\sum_{i=1}^{3}sin(\omega t+\psi_i)+\\&+\frac{\mu_0\sqrt{2}I}{\pi\rho}ak\sum_{n=1}^{\infty}\sum_{i=1}^{3}nI_n^{'}(nka)K_n(nk\rho)sin(\omega t+\psi_i)cos(n(\varphi_{0i}-\varphi+kz))\end{aligned}$$

$$B_z = -\frac{\mu_0\sqrt{2}I}{\pi}ak^2\sum_{n=1}^{\infty}\sum_{i=1}^{3}nI_n^{'}(nka)K_n(nk\rho)sin(\omega t+\psi_i)cos(n(\varphi_{0i}-\varphi+kz))$$

where

$$\sum_{i=1}^{3}sin(\omega t+\psi_i)sin(n(\varphi-\varphi_{0i}-kz)) = \mp\frac{3}{2}cos(\omega t\pm n\Phi) \tag{3.8}$$

$$\sum_{i=1}^{3}sin(\omega t+\psi_i)cos(n(\varphi-\varphi_{0i}-kz)) = \frac{3}{2}sin(\omega t\pm n\Phi) \tag{3.9}$$

$$\sum_{i=1}^{3}sin(\omega t+\psi_i) = 0 \tag{3.10}$$

with $\Phi = \varphi - kz$. It have to be pointed out that the summation (4.4) and (3.9) are zero for $n = 3, 6, 9...$ and not null for all the remain value of n; furthermore, the lower sign applies for $n = 1, 4, 7\ldots$ and the upper for $n = 2, 5, 8\ldots$.

Thus the total effective value of the magnetic field components generated by an infinitely long twisted tripolar cable at observation distances $\rho > a$ are the following:

$$B_\rho(\rho,\varphi,z) = \frac{3\mu_0 I}{2\pi}ak^2\left[\sum_{n=1}^{\infty}\sum_{m=1}^{\infty}\begin{array}{l}(\mp n)(\mp m)I_n^{'}(nka)I_m^{'}(mka)\cdot\\ \cdot K_n^{'}(nk\rho)K_m^{'}(mk\rho)cos((\pm n\mp m)\Phi)\end{array}\right]^{1/2}$$

$$B_\varphi(\rho,\varphi,z) = \frac{3\mu_0 I}{2\pi\rho}ak\left[\sum_{n=1}^{\infty}\sum_{m=1}^{\infty}\begin{array}{l}nmI_n^{'}(nka)I_m^{'}(mka)K_n(nk\rho)\cdot\\ \cdot K_m(mk\rho)cos((\pm n\mp m)\Phi)\end{array}\right]^{1/2} \tag{3.11}$$

$$B_z(\rho,\varphi,z) = \frac{3\mu_0 I}{2\pi}ak^2\left[\sum_{n=1}^{\infty}\sum_{m=1}^{\infty}\begin{array}{l}nmI_n^{'}(nka)I_m^{'}(mka)K_n(nk\rho)\cdot\\ \cdot K_m(mk\rho)cos((\pm n\mp m)\Phi)\end{array}\right]^{1/2}$$

then the magnetic field is [5]

$$B(\rho,\varphi,z) = \sqrt{B_\rho^2+B_\varphi^2+B_z^2} \tag{3.12}$$

These formulations are not simpler than the Biot-Savart integral, on the contrary they are more hard to comprehend conceptually, principally due to the presence of the modified Bessel function of the first $I_\nu(z)$ and the second kind $K_\nu(z)$, but Matlab provide functions that compute directly the results for established argument z and order ν, also their first derivative can be easily calculated by means of the recurrence relations

$$I_\nu^{'}(z) = I_{\nu-1}(z) - \frac{\nu}{z} I_\nu(z) \tag{3.13}$$

$$K_\nu^{'}(z) = -K_{\nu-1}(z) - \frac{\nu}{z} K_\nu(z)$$

thus it is not difficult to implement the programming codes.

Furthermore, the method do not have to compute vector distances or cross products for hundreds or even thousands source points as the Biot-Savart Law, but only dozens orders of the Bessel functions, so the required computational time is reduced a lot. Indeed the functions $I_n^{'}(nka)$, $K_n^{'}(nk\rho)$ and $K_n(nk\rho)$ get to zero quickly with the increase of orders so that the contribution of higher orders can be neglected, in particular it can be observed that: $I_n^{'}(nka)$ is higher with the increasing of the helices radius a and the decreasing of pitch length p, it diverges to infinity for the two cases with $p = 0.8m$, $a = 0.09m$ and $a = 0.1m$ [figure 3.2]; instead $K_n^{'}(nk\rho)$ in absolute values and $K_n(nk\rho)$ are rising for the increase of p and the decrease of the radial distances r, they are divergent for the case with $p = 2m$ and $r = 0.2m$ [figures 3.3 and 3.4]; these functions are compensating each other, because when $I_n^{'}(nka)$ diverges $K_n^{'}(nk\rho)$ and $K_n(nk\rho)$ drop to zero immediately and so on the contrary.

The two extreme cases of the divergence are analysed, with a relative error tolerance set to $10^{-4}\%$ between the magnetic field values calculated by considering consecutive orders n of Bessel functions for the summations, it results that in the case with $p = 0.8m$ and $a = 0.1m$ the method converges for $n = 13$, while in the case of $p = 2m$ and $a = 0.1m$ the convergence order is equal to $n = 19$, even if the maximum error presented at order 13 is already very small (equal to $0.004\mu T$) and the contributions provided by higher orders could be neglected. By making some tests it result that for all other cases the method converge for order around $n = 13$, therefore a cautionary value for the order of Bessel functions set to $n = 50$ is more than enough for the convergence.

The drawback is that the series of the modified Bessel functions cannot provide a correct estimation of the magnetic field, the absolute error can reach order of magnitude of $10^1\mu T$ in the vicinity of the cable and it is approximately $10^{-1}\mu T$ for radial distances above $3m$, where also the magnetic field is almost null; the errors are minor with the decreasing of the helices radius a and the increasing pitch length p, in other word the lower is the magnetic field and the straighter are the cables the less is the error, as the trends of $I_n^{'}(nka)$. Anyway the formulations (3.11) can be adopted only for a fast estimation for an initial feasibility study.

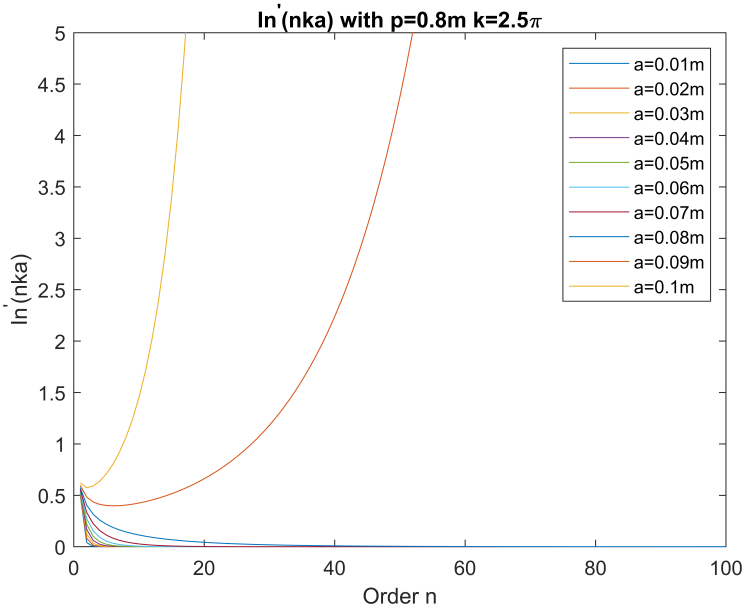

Figure 3.2: $I_n^{'}(nka)$ as a function of the order n with $p = 0.8m$

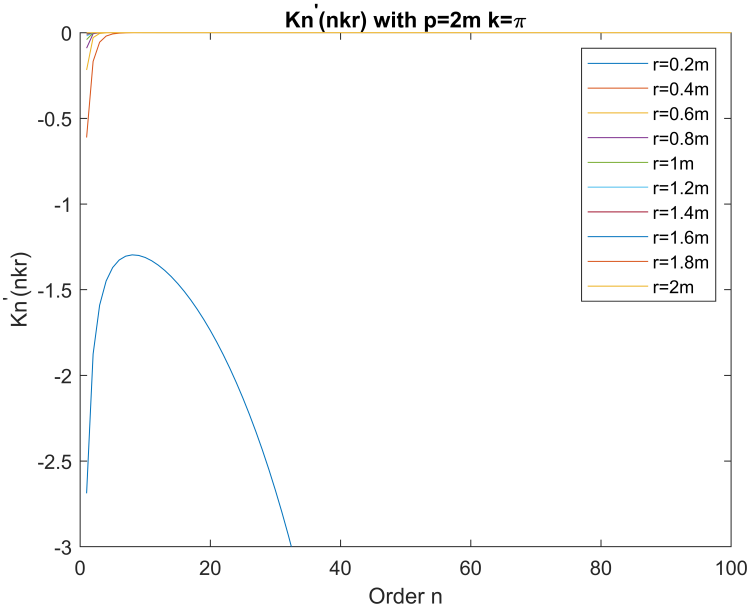

Figure 3.3: $K_n^{'}(nk\rho)$ as a function of the order n with $p = 2m$

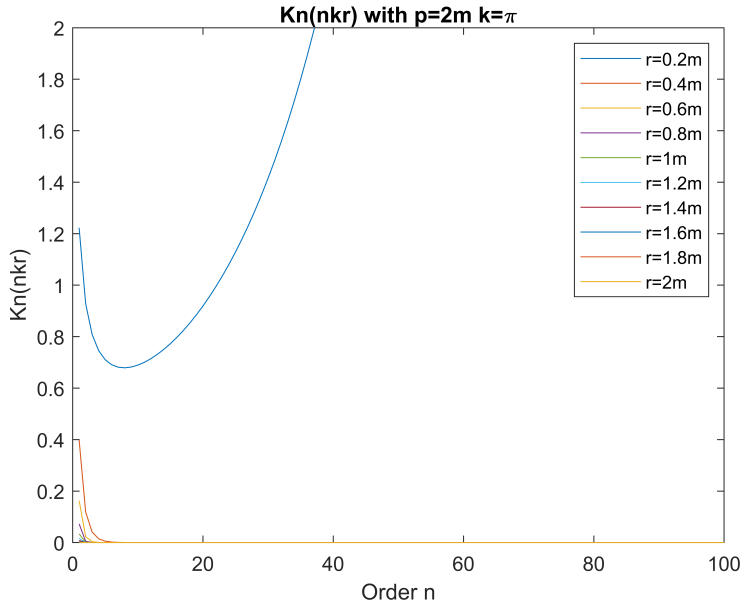

Figure 3.4: $K_n(nk\rho)$ as a function of the order n with $p = 2m$

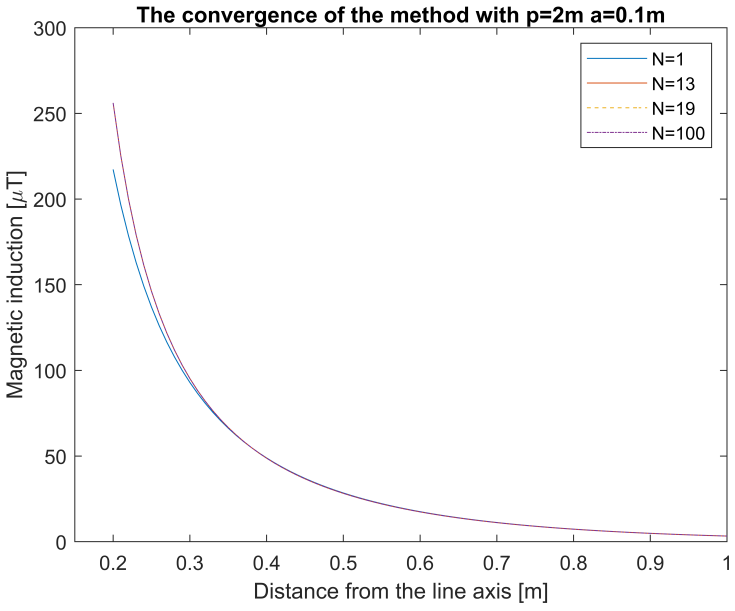

Figure 3.5: the magnetic field at varying orders of Bessel functions

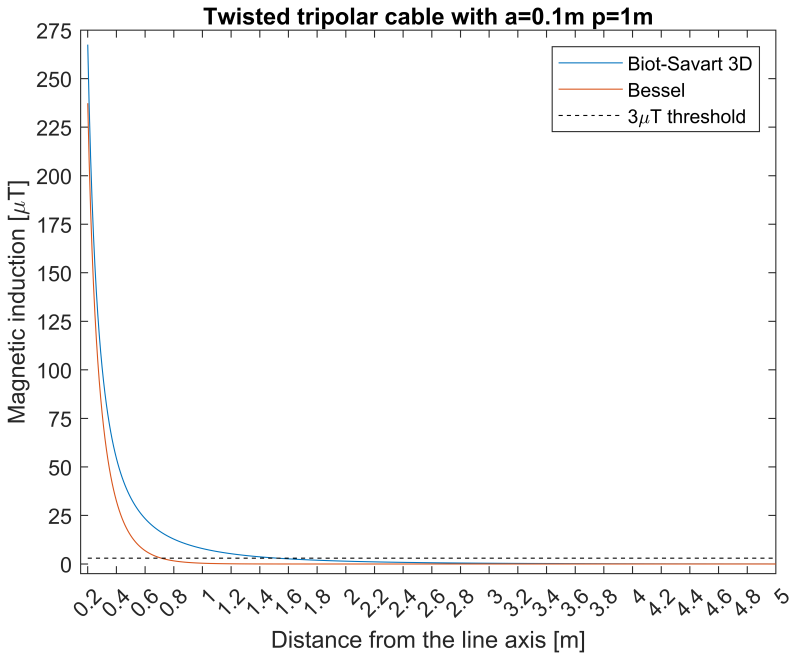

Figure 3.6: The series formulation compared to the Biot-Savart Law
In this case the magnetic field reaches the legislation limits of $3\mu T$ at around $0.7m$, while in the reality it is at distances twice higher (about $1.5m$), therefore a few of additional meters should be reserved in the feasibility study in order to be precautionary.

3.3 Matlab codes

The formulations (3.11) are not implemented as a Matlab function, since in literature are often used its approximations, which will be treated in the next chapters. The script requires only few set data:

1. geometrical parameters describing the helices: the radius a and the pitch length p;

2. parameters indicating the calculation range: the z-coordinate of the considering cross-section, the radial distances r and the angular position θ;

3. about the three-phase currents only the effective value I_{rms} is necessary, instead the currents configuration (phase angle and the angular position on the plane z=0) is not needed.

From these data are derived input arguments and parameters for the calculation of the Bessel functions and the magnetic field; for the first, Matlab functions $besseli(n, nka)$ and $besselk(n, nkr)$, which calculate results of $I_n(nka)$ and $K_n(nkr)$, are used together with the recurrence relations (3.13) into a cycle for; while for the last, each single summands of the double summation in (3.11) is

calculated with two cascading cycles for by considering only three cases instead of five since $cos(\alpha) = cos(-\alpha)$:

1. both lower sign or both upper sign for indices n and m;
2. one index with lower sign and the other with the upper sign;
3. indices equal to 3 and its multiples.

Then, the effective value of the magnetic field components and the total magnetic field is calculated using (3.11) and (3.12).

Listing 3.1: Series formulation (cylindrical coordinates)

```
    % Data
a=0.1;  p=0.8;
z=0;    theta=0;    r=0.2:0.01:5; % [m]
Irms=200; % [A]

    % Data for modified Bessel functions
k=2*pi/p;    eta=k*a;   g=k*r;
N=50; % order of Bessel functions
% indices for lower/upper sign and zero values
low=1:3:N;  up=2:3:N;   zero=3:3:N;

    % Data for the magnetic field
phi=theta-k*z;
muo=4*pi*1e-7*1e6; % Beff expressed in [microT]
Br=zeros(1,length(r));
Bt=zeros(1,length(r));
Bz=zeros(1,length(r));
Btot=zeros(1,length(r));

    % Bessel functions calculation
dIn=zeros(N,1);
Kn=zeros(N,length(r)); dKn=zeros(N,length(r));
for i=1:N
    dIn(i)=besseli(i-1,i*eta)-besseli(i,i*eta)/eta;
    Kn(i,:)=besselk(i,i*g);
    dKn(i,:)=-besselk(i-1,i*g)-Kn(i,:)./g;
end

    % The magnetic field calculation
for j=1:length(r)
    % summands of the series
    Brn=zeros(N,N);  Btn=zeros(N,N);  Bzn=zeros(N,N);
    for n=1:N
        for m=1:N
```

```
            if (any(low==n) && any(low==m)) ||
                (any(up==n) && any(up==m))
                Brn(n,m)=n*m*dIn(n)*dIn(m)*dKn(n,j)*
                         dKn(m,j)*cos((-n+m)*phi);
                Btn(n,m)=n*m*dIn(n)*dIn(m)*Kn(n,j)*
                         Kn(m,j)*cos((-n+m)*phi);
                Bzn(n,m)=n*m*dIn(n)*dIn(m)*Kn(n,j)*
                         Kn(m,j)*cos((-n+m)*phi);
            end
            if (any(low==n) && any(up==m)) ||
               (any(up==n) && any(low==m))
                Brn(n,m)=-n*m*dIn(n)*dIn(m)*dKn(n,j)*
                          dKn(m,j)*cos((-n-m)*phi);
                Btn(n,m)=n*m*dIn(n)*dIn(m)*Kn(n,j)*
                         Kn(m,j)*cos((-n-m)*phi);
                Bzn(n,m)=n*m*dIn(n)*dIn(m)*Kn(n,j)*
                         Kn(m,j)*cos((-n-m)*phi);
            end
            if any(zero==n) && any(zero==m)
                Brn(n,m)=0;  Btn(n,m)=0;  Bzn(n,m)=0;
            end
        end
    end
    % the magnetic field components
    Br(j)=3*muo*Irms*a*k^2/(2*pi)*sqrt(sum(sum(Brn)));
    Bt(j)=3*muo*Irms*a*k/(2*pi*r(j))*
          sqrt(sum(sum(Btn)));
    Bz(j)=3*muo*Irms*a*k^2/(2*pi)*sqrt(sum(sum(Bzn)));
end
% the total magnetic field
Btot=sqrt(Br.^2+Bt.^2+Bz.^2);
```

Chapter 4

Pettersson

4.1 Hagel's formulation simplification

An infinitely long helical line current with phasor $\overline{I}$, radius a and pitch p generates at its outside ($r > a$) a magnetic field with the following radial, azimuthal and axial components (cylindrical coordinates):

$$B_r(r,\varphi,z) = -\frac{\mu_0\overline{I}}{\pi}ak^2\sum_{n=1}^{\infty} nI_n^{'}(nka)K_n^{'}(nkr)sin(n(\varphi_0-\varphi+kz))$$

$$B_\varphi(r,\varphi,z) = \frac{\mu_0\overline{I}}{2\pi r} + \frac{\mu_0\overline{I}}{\pi r}ak\sum_{n=1}^{\infty} nI_n^{'}(nka)K_n(nkr)cos(n(\varphi_0-\varphi+kz)) \quad (4.1)$$

$$B_z(r,\varphi,z) = -\frac{\mu_0\overline{I}}{\pi}ak^2\sum_{n=1}^{\infty} nI_n^{'}(nka)K_n(nkr)cos(n(\varphi_0-\varphi+kz))$$

where $k = 2\pi/p$; I_n and K_n are the modified Bessel functions of first and second kind, $I_n^{'}$ and $K_n^{'}$ their respective first derivative; and φ_0 is the angular position of the intersection point between the helix and the plane $z = 0$[5].

By neglecting the single term of B_φ it results $B_z = -krB_\varphi$, this means that the field component in the φz-plane is perpendicular to an imaginary helix of pitch p passing through the observation point, then considering the natural coordinates with the tangential B_s, the binormal B_b and the normal B_n components defined as follow

$$\begin{aligned} B_s &= B_z\sin\Psi + B_\varphi\cos\Psi \\ B_b &= B_z\cos\Psi - B_\varphi\sin\Psi \\ B_n &= -B_r \end{aligned} \quad (4.2)$$

where $\Psi = \arctan(kr)$ is the pitch angle of the imaginary helix, the magnetic field is described by only two components, the radial and the binormal ones,

since the tangential component is null

$$B_r = -\frac{\mu_0 \overline{I}}{\pi} ak^2 \sum_{n=1}^{\infty} nI_n^{'}(nka)K_n^{'}(nkr)sin(n(\varphi_0 - \varphi + kz)) \tag{4.3}$$

$$B_b = -\frac{\mu_0 \overline{I}}{\pi r} ak\sqrt{1+(kr)^2} \sum_{n=1}^{\infty} nI_n^{'}(nka)K_n(nkr)cos(n(\varphi_0 - \varphi + kz))$$

where the cylindrical coordinates are retained for the radial field component and the observation points.

For the three-phase configuration, the i-th line current intersects the plane $z = 0$ at angular position φ_{0i} and the correspondent i-th circulating current I_i is expressed with time dependent formulations, where $i = 1, 2, 3$

$$\varphi_{0i} = (i-1)\frac{2\pi}{3} \quad I_i = \sqrt{2}I\sin(\omega t + \psi_i) = \sqrt{2}I\sin\left(\omega t + (i-1)\frac{2\pi}{3}\right)$$

By considering the expressions below derived from the trigonometric properties

$$\sum_{i=1}^{3} sin(\omega t + \psi_i)sin(n(\varphi - \varphi_{0i} - kz)) = \mp\frac{3}{2}cos(\omega t \pm n\Phi) \tag{4.4}$$

$$\sum_{i=1}^{3} sin(\omega t + \psi_i)cos(n(\varphi - \varphi_{0i} - kz)) = \frac{3}{2}sin(\omega t \pm n\Phi)$$

the magnetic field components as the sum of contributions from the three currents are as a function of the time

$$B_r = \frac{3\mu_0\sqrt{2}I}{2\pi} ak^2 \sum_{n=1}^{\infty} (\mp n)I_n^{'}(nka)K_n^{'}(nkr)cos(\omega t \pm n\Phi) \tag{4.5}$$

$$B_b = -\frac{3\mu_0\sqrt{2}I}{2\pi r} ak\sqrt{1+(kr)^2} \sum_{n=1}^{\infty} nI_n^{'}(nka)K_n(nkr)sin(\omega t \pm n\Phi)$$

where $\Phi = \varphi - kz$. It is recalled that the summations range over all positive integers except $n = 3, 6, 9\ldots$ and the lower sign applies for $n = 1, 4, 7\ldots$ while the upper for $n = 2, 5, 8\ldots$.

The effective values of the two components and the total magnetic field result [6]

$$B_r = \frac{3\mu_0 I}{2\pi} ak^2 \left[\sum_{n=1}^{\infty}\sum_{m=1}^{\infty} \begin{array}{l}(\mp n)(\mp m)I_n^{'}(nka)I_m^{'}(mka)\cdot \\ \cdot K_n^{'}(nkr)K_m^{'}(mkr)cos((\pm n \mp m)\Phi)\end{array}\right]^{1/2}$$

$$B_b = \frac{3\mu_0 I}{2\pi r} ak\sqrt{1+(kr)^2} \left[\sum_{n=1}^{\infty}\sum_{m=1}^{\infty} \begin{array}{l}nmI_n^{'}(nka)I_m^{'}(mka)K_n(nkr)\cdot \\ \cdot K_m(mkr)cos((\pm n \mp m)\Phi)\end{array}\right]^{1/2} \tag{4.6}$$

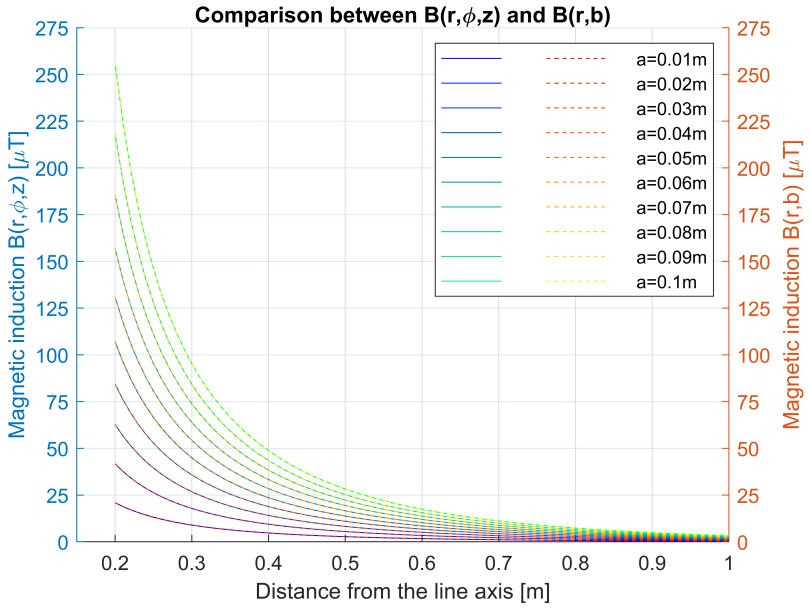

Figure 4.1: Comparison between the natural and the cylindrical formulations

$$B = \sqrt{B_r^2 + B_b^2}$$

The formulation in the natural coordinates is analogous to the one in the cylindrical coordinates, they provide the same results and all the considerations made for the three-phase version of the Hagel's formulation in the previous chapter are valid also for (4.6), therefore these latest formulations is more advantageous, because it speeds up computational time while maintaining the results, since it nullifies one component and reduces the calculation to two dimension just rotating the reference axes.

4.2 Series expansions reduction

In the previous chapter were shown graphs of the functions $I_n^{'}(nka)$, $K_n^{'}(nkr)$ and $K_n(nkr)$, it can can be summarized that their values are higher at low terms and drop to zero quickly with the increase of order n (except three borderline cases), in particular when the cable has a loose twist configuration so that the helices radius is much smaller than the pitch length $a << p$, and the observation point is taken at far distances much greater than the pitch length $r >> p$, the first terms are so dominant that all the subsequent addends of the series expansions could be neglected, therefore the formulations (4.6) become

$$B_{r1} = \frac{3\mu_0 I}{2\pi} a k^2 I_1'(ka) K_1'(kr) \tag{4.7}$$

$$B_{b1} = \frac{3\mu_0 I}{2\pi r} ak\sqrt{1+(kr)^2} I_1'(ka) K_1(kr)$$

and as result the effective total field value can be quite simplified [6]

$$B_1 = \sqrt{B_r^2 + B_b^2} = \frac{3\mu_0 I}{2\pi} ak^2 I_1'(ka) \left[K_1'^2(kr) + \frac{1+(kr)^2}{(kr)^2} K_1^2(kr) \right]^{1/2} \tag{4.8}$$

But it have to be evaluated the range of the ratios a/p and r/p within which the terms of higher orders could be actually neglected and the results of the reduced series considered still valid. The formulations (4.6) is implemented with Bessel orders equal to $N = 50$ in comparison with (4.8); and the considered values for parameters are $a = 0.01 \div 0.1m$, $p = 0.8, 1.2, 1.6, 2m$ and $r = 0.2 \div 5m$. In the table 4.1 are listed the minimum value of a above which the effective total field $B_1(r, b)$ obtained from (4.8) presents relative errors higher than 1% respect to $B_{50}(r, b)$ obtained from (4.6), it can be noted that generally the errors rise for higher a and lower r with fixed p, in particular for $a/p > 0.1$ and $r/p < 0.25$; good field estimation is provided for $a < 0.1p$ and $r > 0.3m$ for $p = 0.8 \div 2m$, but if lower r/p is wanted to be considered the limits for a/p have to be lowered too; for the radial distances of practical interests the reduced series presents the same results as the complete formulation.

Table 4.1: Borderline cases of the reduced series with relative errors above 1%

	$r = 0.2m$			$r = 0.3m$		
p $[m]$	r/p	a_{min} $[m]$	a_{min}/p	r/p	a_{min} $[m]$	a_{min}/p
0.8	0.25	0.08	0.1	0.375	/	/
1.2	0.1667	0.06	0.05	0.25	/	/
1.6	0.125	0.06	0.0375	0.1875	0.1	0.0625
2	0.1	0.05	0.025	0.15	0.09	0.045

4.3 Further approximations

Since (4.8) contains still three Bessel functions, Pettersson made further simplifications by considering the small argument approximation for the modified Bessel function of the first kind and the large argument approximation for the second kind

$$I_1'(ka) \approx \frac{1}{2} \quad for\ \frac{a}{p} << 1\ (loose\ twist) \tag{4.9}$$

$$K_1(kr) \approx -K_1'(kr) \approx \sqrt{\frac{\pi}{2kr}} e^{-kr} \quad for\ \frac{r}{p} >> 1\ (far\ distances)$$

so the final formulation he obtained is

$$B_1 \approx \frac{3}{4} \frac{\mu_0 I a k^2}{\pi} \sqrt{\frac{\pi}{2kr}} e^{-kr} \sqrt{\frac{1+2(kr)^2}{(kr)^2}} \approx \frac{3}{4} \frac{\mu_0 I a k^2}{\sqrt{\pi}} \frac{e^{-kr}}{\sqrt{kr}} \tag{4.10}$$

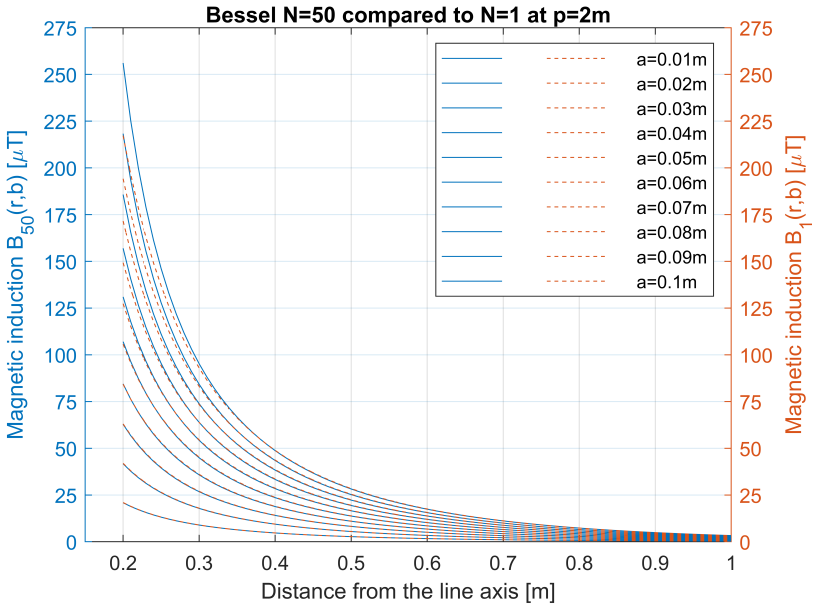

Figure 4.2: Comparison between $B_1(r,b)$ and $B_{50}(r,b)$ at fixed $p = 2m$
At $r = 0.2m$ the error rise from 1% at $a = 0.05m$ up to 15.16% at $a = 0.1m$, which is the highest error among all the considered cases, but it is principally due to the low $r/p = 0.1$ since $a/p = 0.025 \div 0.05 < 0.1$; at $r = 0.3m$ with $a = 0.1m$ the error is reduced to 2.38%; above $0.4m$ errors are all under 1% and the reduced series could represents a nice simple method for the magnetic field estimation.

where the second term under the square root could be approximated to $\sqrt{2}$, since $kr = 2\pi r/p >> 1$[6].

As previously done for the reduced series, the same evaluation on the validation range of the ratios a/p and r/p is made. It results that there are borderline cases with $p = 0.8m$ and $a = 0.07 \div 0.1m$ that present relative errors always higher than 10% respect to $B_{50}(r,b)$, because the Pettersson's formulation runs to zero at lower radial distances due to the approximations, therefore the maximum admissible relative error is set to 10%. From the table 4.2, where are listed the limiting value of a for $p = 0.8, 1.2, 1.6, 2m$ and $r = 0.2, 1, 5m$, it results that the errors are higher than 10% for $a/p > 0.0875$ and $r/p < 6.25$.

4.4 Matlab codes

For briefness of the codes some parameters are introduced:

$$B_0 = \frac{\mu_0 I a}{\pi r^2} \qquad \eta = ka = \frac{2\pi a}{p} \qquad \gamma = kr = \frac{2\pi r}{p} \tag{4.11}$$

Therefore the formulations (4.6), (4.8) and (4.10) are rewritten as follows:

Table 4.2: Pettersson's borderline cases with relative errors above 10%

	$r = 0.2m$			$r = 1m$			$r = 5m$		
p $[m]$	r/p	a_{min} $[m]$	a_{min}/p	r/p	a_{min} $[m]$	a_{min}/p	r/p	a_{min} $[m]$	a_{min}/p
0.8	0.25	0.01	0.0125	1.25	0.04	0.05	6.25	0.07	0.0875
1.2	0.1667	0.01	0.0083	0.8333	0.01	0.0083	4.1667	0.09	0.075
1.6	0.125	0.01	0.0063	0.625	0.01	0.0063	3.125	/	/
2	0.1	0.01	0.005	0.5	0.01	0.005	2.5	/	/

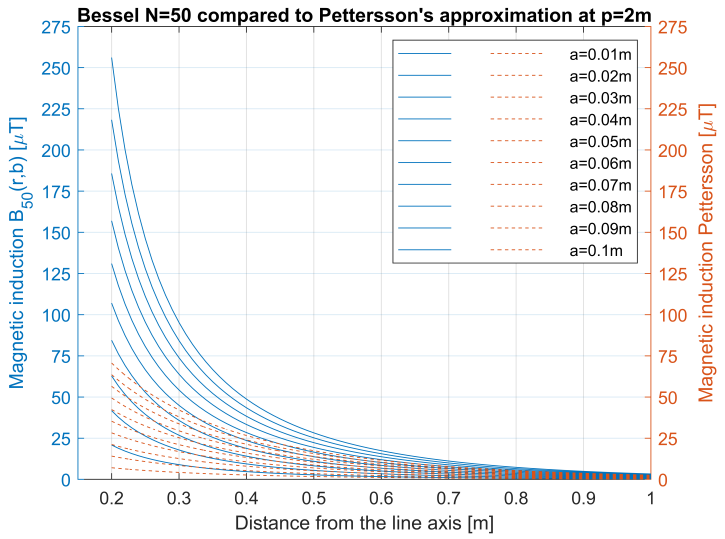

Figure 4.3: Comparison between Pettersson and $B_{50}(r, b)$ at fixed $p = 2m$
At $r = 0.2m$ there are the highest errors that ranges from 66% ($a = 0.01m$) up to 72% ($a = 0.1m$), principally due to the low $r/p = 0.1$ since $a/p = 0.005 \div 0.05 < 0.0875$; at $r = 1m$ the errors are still around 20%; the errors result minor than 10% only for $r > 3m$.

- the two-dimensional series formulation

$$B_r = \frac{3}{2} B_0 \gamma^2 \left[\sum_{n=1}^{\infty} \sum_{m=1}^{\infty} (\mp n)(\mp m) I_n'(n\eta) I_m'(m\eta) \cdot \right. \\ \left. \cdot K_n'(n\gamma) K_m'(m\gamma) cos((\pm n \mp m)\Phi) \right]^{1/2}$$

$$B_b = \frac{3}{2} B_0 \gamma \sqrt{1+\gamma^2} \left[\sum_{n=1}^{\infty} \sum_{m=1}^{\infty} nm I_n'(n\eta) I_m'(m\eta) K_n(n\gamma) \cdot \right. \\ \left. \cdot K_m(m\gamma) cos((\pm n \mp m)\Phi) \right]^{1/2} \tag{4.12}$$

$$B = \sqrt{B_r^2 + B_b^2}$$

- the series reduced to order N=1

$$B_1 = \frac{3}{2} B_0 \gamma^2 I_1'(\eta) \left[K_1'^2(\gamma) + \frac{1+\gamma^2}{\gamma^2} K_1^2(\gamma) \right]^{1/2} \tag{4.13}$$

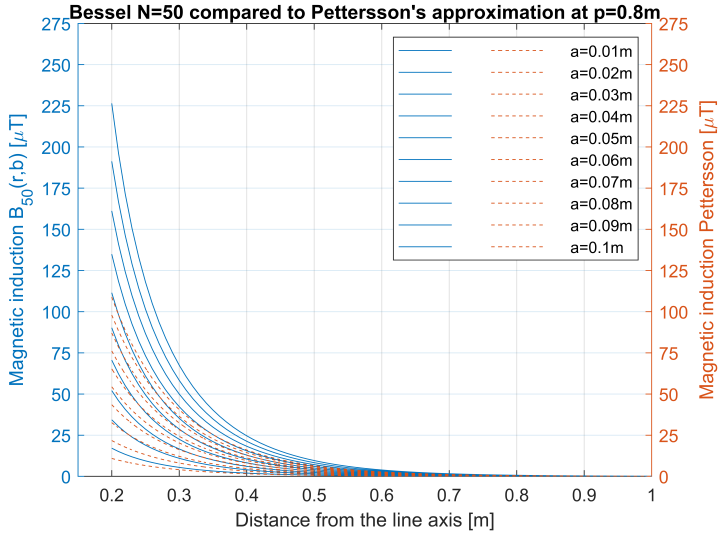

Figure 4.4: Comparison between Pettersson and $B_{50}(r, b)$ at fixed $p = 0.8m$
In this case the errors at $r = 0.2m$ are lower ($36 \div 52\%$), because the ratio $r/p = 0.25$ is higher respect to $p = 2m$, but at $r = 1m$ the errors are still around 20% for $a = 0.06 \div 0.1m$, because the ratio a/p is closer or even higher respect to the limit of 0.0875.

- the Pettersson's formulation

$$B_1 \approx \sqrt{\frac{\pi}{2}}\gamma^{3/2}e^{-\gamma} \cdot \frac{3}{4}\sqrt{2}B_0 = F \cdot \frac{3}{4}\sqrt{2}B_0 \tag{4.14}$$

The two-dimensional series formulation is codified as a function called Bessel3F, because it is taken as reference for the other two simplified methods and also for the Landini's formulation which will be exposed in the next chapter. It requires six inputs:

1. the helices geometrical parameters: the radius a and the pitch length p;
2. the calculation area: described by the radial distances r and the angular position $\Phi = \theta - kz$;
3. the order of the Bessel functions N, which coincides with the upper bound of the summations;
4. the effective value of the balanced three-phase currents I.

It calculate with the variation of a and p the effective values of the magnetic field and its two components for all the considered radial distances and saves the results in three three-dimensional matrices. The calculation steps follow the same logic implemented with the three-phase version of the Hagel's formulation explained in the previous chapter.

Listing 4.1: Series formulation (natural coordinates)

```
function [B]=Bessel3F(a,p,r,N,phi,I)
    % Data
muo=4*pi*1e-7*1e6; % Beff expressed in [microT]
k=2*pi./p;

eta=zeros(length(a),length(p));
Bo=zeros(length(a),length(r));
for i=1:length(a)
    eta(i,:)=k*a(i);
    Bo(i,:)=muo*I*a(i)./(pi*r.^2);
end
gamma=zeros(length(p),length(r));
for i=1:length(p)
    gamma(i,:)=k(i)*r;
end

    % Calculation
B=zeros(length(a),length(r),length(p));
Br=zeros(length(a),length(r),length(p));
Bb=zeros(length(a),length(r),length(p));
% indices for lower / upper sign and zero values
down=1:3:N;  up=2:3:N;  zero=3:3:N;

for ia=1:length(a)
for ip=1:length(p)
    dIn=zeros(N,1);
    Kn=zeros(N,length(r)); dKn=zeros(N,length(r));
    for i=1:N
        dIn(i)=besseli(i-1,i*eta(ia,ip))-
               besseli(i,i*eta(ia,ip))/eta(ia,ip);
        Kn(i,:)=besselk(i,i*gamma(ip,:));
        dKn(i,:)=-besselk(i-1,i*gamma(ip,:))-
                  Kn(i,:)./gamma(ip,:);
    end
    for ir=1:length(r)
        Brn=zeros(N,N);  Bbn=zeros(N,N);
        for n=1:N
        for m=1:N
            if (any(down(:)==n) && any(down(:)==m)) ||
                (any(up(:)==n) && any(up(:)==m))
                Brn(n,m)=n*m*dIn(n)*dIn(m)*dKn(n,ir)*
                         dKn(m,ir)*cos((-n+m)*phi);
                Bbn(n,m)=n*m*dIn(n)*dIn(m)*Kn(n,ir)*
                         Kn(m,ir)*cos((-n+m)*phi);
```

```
            end
            if (any(down(:)==n) && any(up(:)==m)) ||
               (any(up(:)==n) && any(down(:)==m))
                Brn(n,m)=-n*m*dIn(n)*dIn(m)*dKn(n,ir)*
                          dKn(m,ir)*cos((-n-m)*phi);
                Bbn(n,m)=n*m*dIn(n)*dIn(m)*Kn(n,ir)*
                         Kn(m,ir)*cos((-n-m)*phi);
            end
            if any(zero==n) && any(zero==m)
                Brn(n,m)=0;  Bbn(n,m)=0;
            end
        end
        end
        Br(ia,ir,ip)=3/2*Bo(ia,ir)*gamma(ip,ir)^2*
                     sqrt(sum(sum(Brn)));
        Bb(ia,ir,ip)=3/2*Bo(ia,ir)*gamma(ip,ir)*
                     sqrt(1+gamma(ip,ir)^2)*
                            sqrt(sum(sum(Bbn)));
    end
end
end
    B=sqrt(Br.^2+Bb.^2);
end
```

The reduced series and the Pettersson's formulations require the same parameters and save the effective field values in three-dimensional matrices just as the function Bessel3F.

Listing 4.2: Pettersson's approximation

```
    %% Data
muo=4*pi*1e-7*1e6; % Beff expressed in [microT]
I=200; % rms value [A]

a=0.01:0.01:0.1;
p=0.8;
r=0.2:0.01:1;
z=0;   theta=0;

k=2*pi./p;   phi=theta-kz;
eta=zeros(length(a),length(p));
Bo=zeros(length(a),length(r));
for i=1:length(a)
    eta(i,:)=k*a(i);
    Bo(i,:)=muo*I*a(i)./(pi*r.^2);
end
g=zeros(length(p),length(r));
```

```
for i=1:length(p)
    g(i,:)=k(i)*r;
end

    %% Bessel order 1
% hp a<<p & r>>p -> neglect all higher orders

B1=zeros(length(a),length(r),length(p));
for ia=1:length(a)
    for ip=1:length(p)
        I1=besseli(1,eta(ia,ip));
        K1=besselk(1,g(ip,:));
        dI1=besseli(0,eta(ia,ip))-I1/eta(ia,ip);
        dK1=-besselk(0,g(ip,:))-K1./g(ip,:);

    B1(ia,:,ip)=3/2*Bo(ia,:).*g(ip,:).^2*dI1.*
       sqrt(dK1.^2+(1+g(ip,:).^2)./g(ip,:).^2.*K1.^2);
    end
end

    %% Pettersson's approximations
Bpett=zeros(length(a),length(r),length(p));
for ia=1:length(a)
    for ip=1:length(p)
        F=sqrt(pi/2).*g(ip,:).^(3/2).*exp(-g(ip,:));
        Bpett(ia,:,ip)=F*3/4*sqrt(2).*Bo(ia,:);
    end
end
```

Chapter 5

Landini

5.1 Landini's parametric equation

As mentioned in the previous chapters the Biot-Savart Law provide a correct estimation of the magnetic field generated by a finite twisted tripolar cable, but it takes too long computational time; the series formulation that considers three infinitely long helical line currents contains modified Bessel functions and their derivatives, that make its application difficult although the calculation speed is reduced; the simplified formulations proposed by Pettersson, that consist in keeping only the first order of the Bessel functions as an approximation for the whole series, give good estimations only for far distances and loose twist, otherwise the errors respect the infinite series are very high. Therefore Landini thought to carry out a heuristic parametric analysis based on the approximation to the first two terms for the infinite series, because he deducted from a convergence analysis that for distances greater than $1m$ the two-terms solution constitute a very good approximation that always overestimates the series.

The series formulation is re-elaborated by replacing the whole square root with a function A_2

$$A_2 = \left[\sum_{n=1}^{2} \sum_{m=1}^{2} nm I_n^{'}(nka) I_m^{'}(mka) \left((\mp 1)(\mp 1) K_n^{'}(nkr) K_m^{'}(mkr) + \right. \right. \\ \left. \left. + \frac{1 + (kr)^2}{(kr)^2} K_n(nkr) K_m(mkr) \right) \cos((\pm n \mp m)\Phi) \right]^{1/2} \tag{5.1}$$

$$B \approx B_2 = \frac{3\mu_0 I}{2\pi} a k^2 A_2 = \frac{3(4\pi 10^{-7}) Ia}{2\pi} \left(\frac{2\pi}{p} \right)^2 A_2 \cdot 10^{-6} = 2.4\pi^2 \frac{a}{p^2} I \cdot A_2 \tag{5.2}$$

where B_2 is multiplied for 10^{-6} so that it directly results in $[\mu T]$. It can be observed that only the function A_2 determines the dependence of the magnetic field on the radial distance r; and by representing the graph of the field B_2 as a function of r on a semi-logarithmic scale, it can be noted that it is almost all

linear with a slight hyperbolic deviation at small values of r, thus the logarithm of the function A_2 can be approximated with an equation of a line at which it is added a hyperbolic term that quickly goes to zero for the increasing of r:

$$ln(A_2) = a_0 + a_1 r + \frac{a_2}{r^{a_3}} \tag{5.3}$$

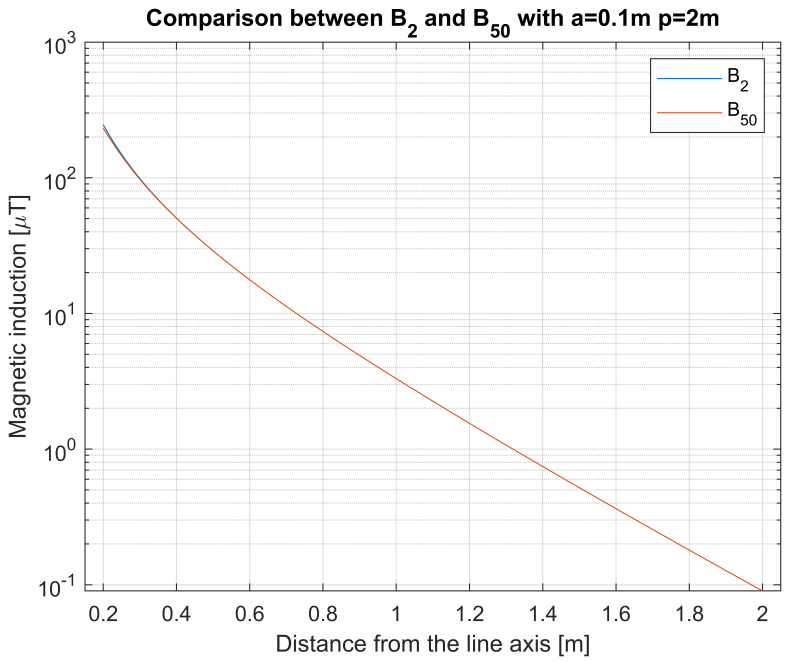

Figure 5.1: Example case of 2-terms series compared to 50-terms series
B_2 almost coincides with B_{50} along r, it presents small overestimation only in the close proximity of the twisted cable (that is advantageous); moreover the magnetic field is principally linear with a curvature at low distances.

The parametric equation for the magnetic field results

$$ln(B) \approx ln(B_2) = ln\left(2.4\pi^2 \frac{a}{p^2} I A_2\right) = ln(G) + ln(I) + a_0 + a_1 r + \frac{a_2}{r^{a_3}} \tag{5.4}$$

where the field is still directly proportional to the current I, the dependence on r is approximated by A_2 and the dependence on the geometrical characteristics (radius a and pitch p) is expressed clearly by the constant $G = 2.4\pi^2 a/p^2$ and roughly by the parameters a_0, a_1, a_2 and a_3 of the function A_2.

To calculate the parameters, Landini considered essential to determine with precision the values of the a_0 and a_1 that govern the linear part, which concerns the calculation range of more practical interest for the human exposure. Secondarily the calculation of a_2 and a_3 is made by attempt to minimise the

overall error, after some tests it is established to maintain constant $a_2 = 0.1$, while a_3 is calculated by considering the linearity from $r = 1.2m$ to $2m$, so that the errors are minimized favouring at the same time the overestimation (anyway not higher than10%).

The results obtained are ordered in lookup tables as a functions of the helix radius $a = 0.01 \div 0.1m$ and the pitch length $p = 0.8 \div 2$; as the second step polynomial expressions are derived to approximate the dependence of the parameters on a and p, in particular it is find that a_0 is a second-degree function of both a and p, a_1 is a third-degree function of p and is not dependent on a, a_3 is a linear function of both a and p:

$$\begin{aligned} a_0(a,p) = &\left[12.8712a^2 + 0.2107a - 0.1383\right] p^2 + \\ &+ \left[-48.4318a^2 - 0.6919a + 0.9094\right] p + \\ &+ \left[49.6932a^2 + 0.5724a - 1.3991\right] \end{aligned} \tag{5.5}$$

$$a_1 = 2.1018p^3 - 11.6186p^2 + 23.2879p - 20.4446 \tag{5.6}$$

$$a_3 = (0.2739a + 0.2430)p + 0.1036a + 1.4444 \tag{5.7}$$

The Landini's parametric formulation (5.4) is implemented with the polynomial functions (5.5÷5.7) and examples of results are shown in figures 5.2 and 5.3. Actually for r above $0.8m$ it provides good estimation of the magnetic field without excessive overestimation and the errors are always lower than the Pettersson's approximation; but for radial distances minor than $0.4m$ the errors could reach at a maximum of around 65% with $a = 0.1m$ at $r = 0.2m$, anyway it is still lower respect to those presented by Pettersson that is equal to 70%; instead for distances between $0.3 \div 0.8m$ the field is underestimated, however the errors are really small and perfectly admissible. This considerations are valid for all other values of $p = 0.8 \div 2m$, the only difference is that the errors are generally reduced with the decreasing of p, in particular the maximum error presented for $p = 0.8m$ is equal to 40% (with $a = 0.1m$ at $r = 0.2m$), against the 50% of the Pettersson's approximation.

It can be said that even if the parametric formulation has a more complex expression than the Pettersson's one, it is nevertheless considerably simplified with respect to the series expansions, since it is composed by polynomials with at most 3 degree, instead of the complex Bessel functions and their derivatives. Anyway its greater complexity compared to the Pettersson's formulation is justified by its better performance on the magnetic field evaluation[1].

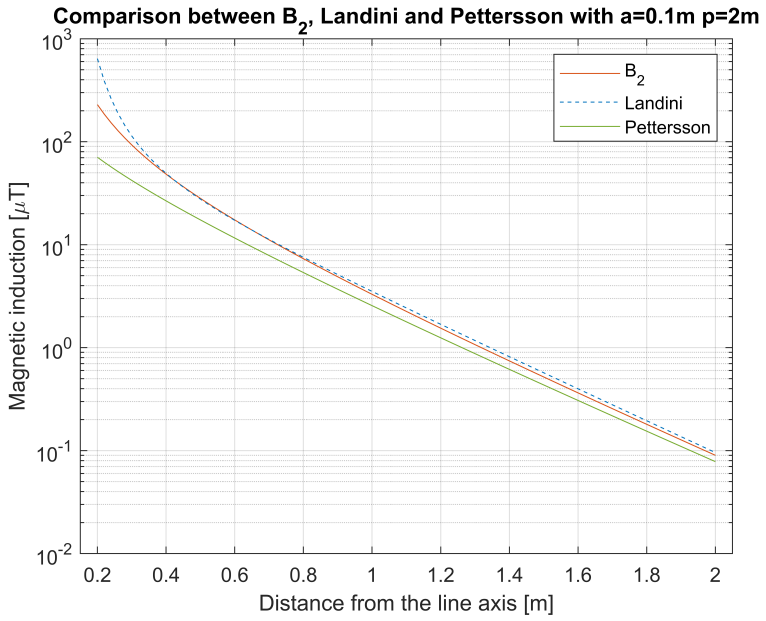

Figure 5.2: Example case: $p = 2m$ $a = 0.1m$

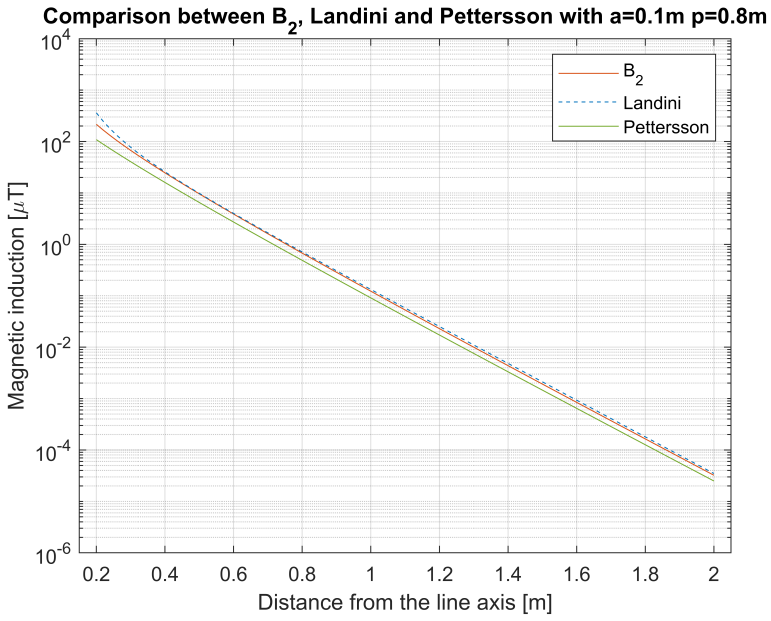

Figure 5.3: Example case: $p = 0.8m$ $a = 0.1m$

5.2 Landini's method applied on Biot-Savart

Since the series expansion present not negligible errors respect to the Biot-Savart integral, it is decided to adopt the same heuristic method based on the results of the three-dimensional Biot-Savart formulation by means of the Matlab Curve Fitter application.

The graphs on the semi-logarithmic scale of the magnetic field obtained with the Biot-Savart Law are still meanly linear with smalls deviations near to the twisted cable, but it goes to zero slowly, not as the Bessel functions series that drop quickly to zero, so the linear part present a minor slope; also, the hyperbolic part present a greater curvature with a steeper increase at low distances. Therefore one degree is added to the numerator of the hyperbolic equation and one quadratic term is added to the linear equation in order to enlarge the curved part

$$A_{new} = a_0 + a_1 r + a_2 r^2 + \frac{a_3 + a_4 r}{r^{a_5}} \tag{5.8}$$

$$ln(B_{new}) = ln\left(2.4\pi^2 \frac{a}{p^2}\right) + ln(I) + A_{new} \tag{5.9}$$

where it results from testing that for $a_3 = 40$ the magnetic field curves are well fitted, while all other parameters are dependent on a and p (the obtained lookup tables are in the appendices of this chapter).

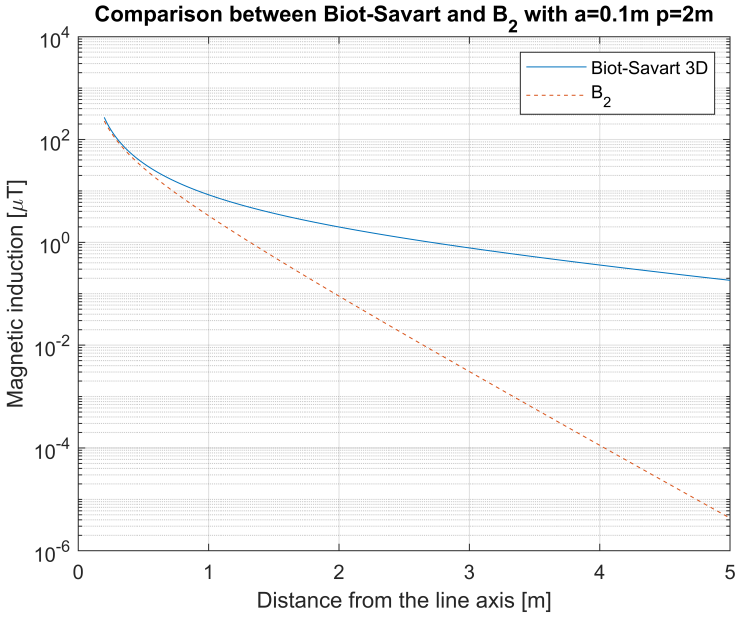

Figure 5.4: Example case of 2-terms series compared to Biot-Savart Law

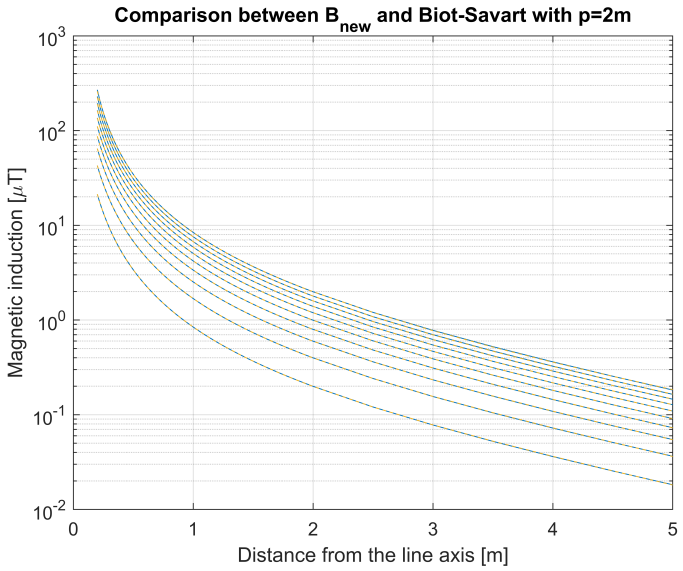

Figure 5.5: B_{new} compared to Biot-Savart with $p = 2m$ $a = 0.01 \div 0.1m$
The blue solid lines are the Biot-Savart results and the yellow dashed lines are the results of the parametric equation B_{new}, which are perfectly stacked on the blue lines.

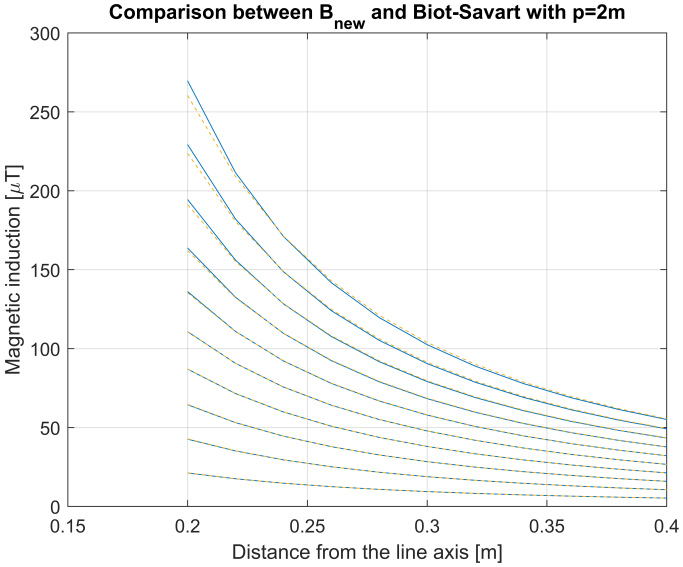

Figure 5.6: B_{new} compared to Biot-Savart with $p = 2m$ $a = 0.01 \div 0.1m$
At very close distances ($r = 0.2 \div 0.4m$), the parametric equation underestimate a little bit the field, but the errors are very small (around 3%)

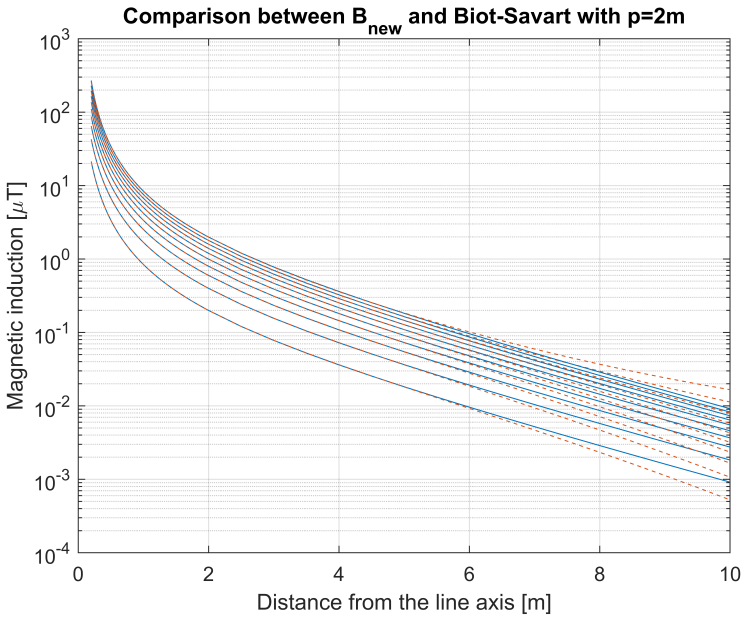

Figure 5.7: B_{new} compared to Biot-Savart with $p = 2m$ $a = 0.01 \div 0.1m$

It should be stressed out that the parametric equation (5.9) with the tabulated parameters in the appendices works only until $r = 5m$, outside this range of the distances the curves diverge due to those added terms. The field is overestimated for the cases with $a = 0.08 \div 0.1m$, but for lower a it is underestimated, although at $r = 5m$ the field is of the order of magnitude around $10^{-1}\mu T$, so the uncertainty presents on the second decimal place and beyond, thus the absolute error is very small.

Once obtained the exact values of the parameters, these have to be expressed as functions of the helix radius a and the pitch p, By observing the graphics of the parameters separately for varying of a and p, the relationship between them can be deduced, then an approximated polynomial equation can be obtained by means of the Matlab Curve Fitter application. It is thought to not exceed the polynomials over 3 degrees in order to avoid too long and complex formulations.

5.2.1 The parameter a_0

The parameter a_0 is a two-degree function of both the helix radius a and the pitch p, therefore it could be approximated as

$$a_0 \approx c_{00} + c_{10} \cdot p + c_{01} \cdot a + c_{20} \cdot p^2 + c_{11} \cdot pa + c_{02} \cdot a^2 \tag{5.10}$$

where the coefficients are automatically calculated by Matlab obtaining

$$a_0 \approx -47.85 + 4.301p + 2.21a - 0.8089p^2 + 1.17pa - 143.7a^2 \tag{5.11}$$

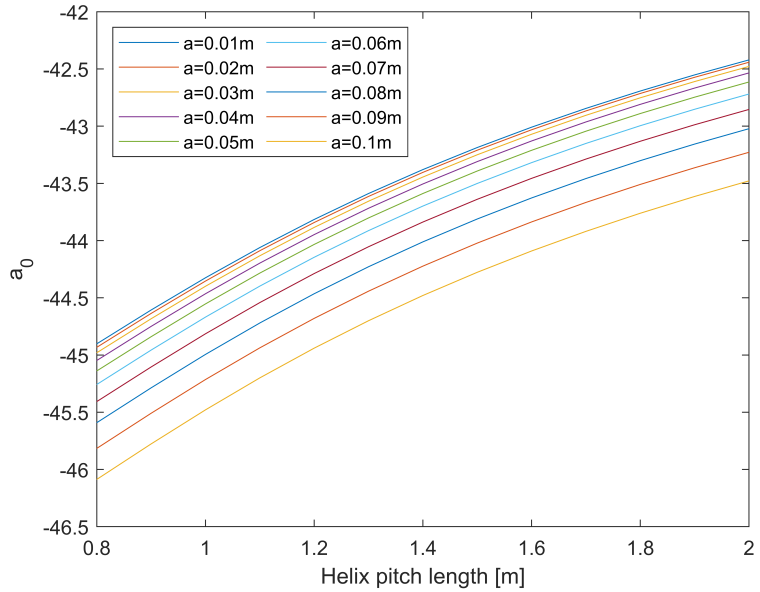

Figure 5.8: The parameter a_0 as a function of p

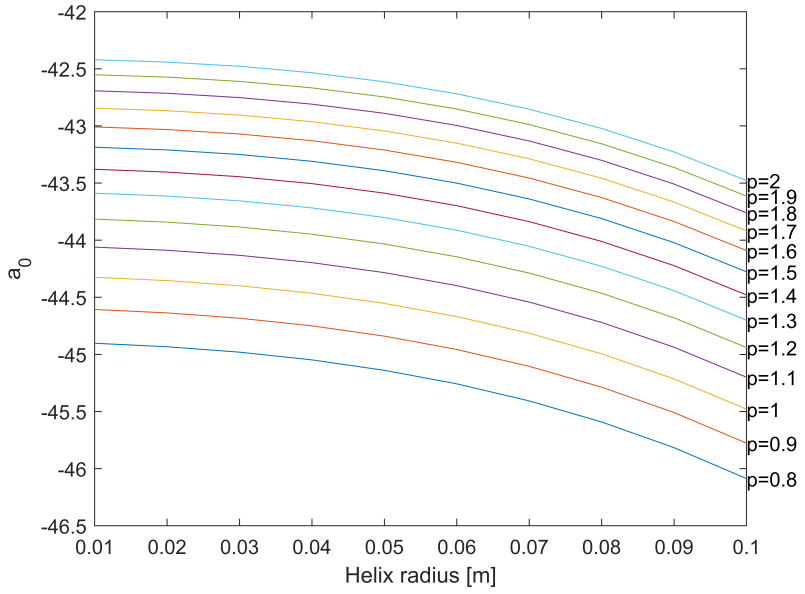

Figure 5.9: The parameter a_0 as a function of a

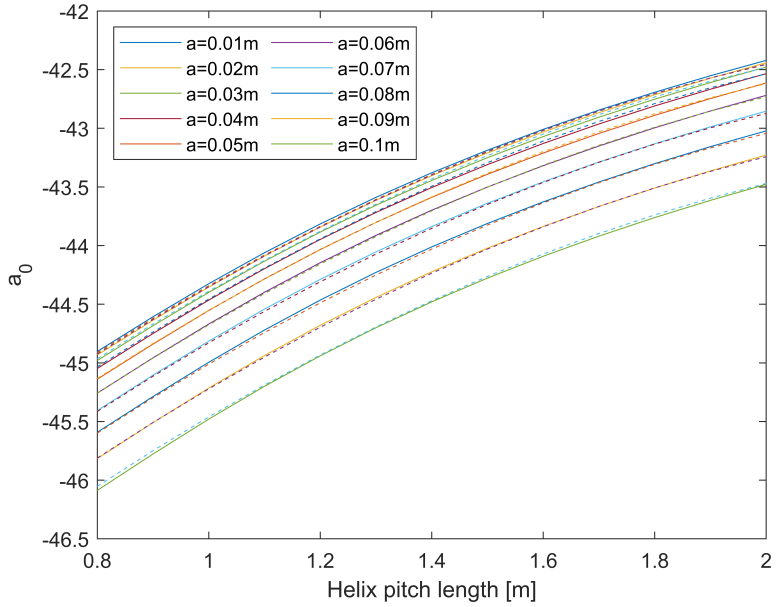

Figure 5.10: The parameter a_0 and its approximation as a function of p

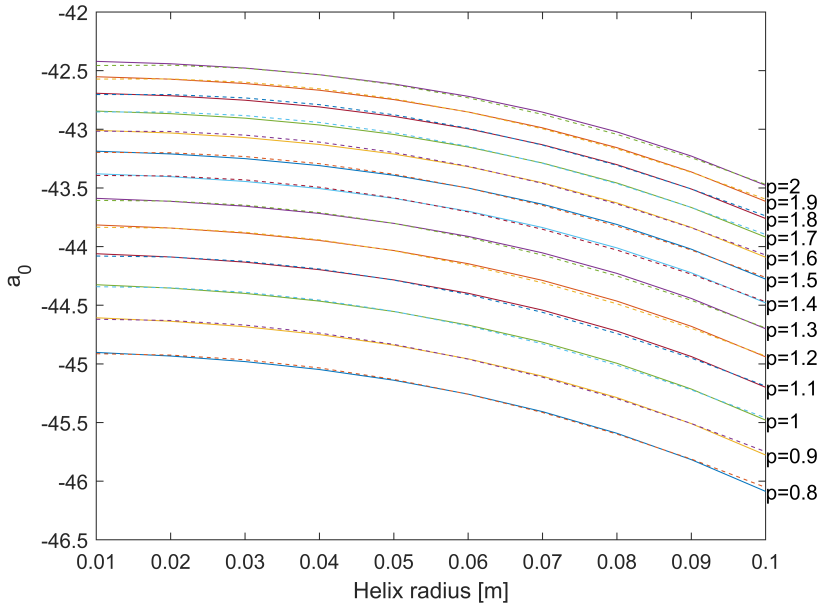

Figure 5.11: The parameter a_0 and its approximation as a function of a

5.2.2 The parameter a_1

The parameter a_1 has a quadratic dependence on both the helix radius a and the pitch p as well

$$a_1 \approx -34.35 + 32.2p + 41.63a - 7.11p^2 - 23.54pa - 1013a^2 \tag{5.12}$$

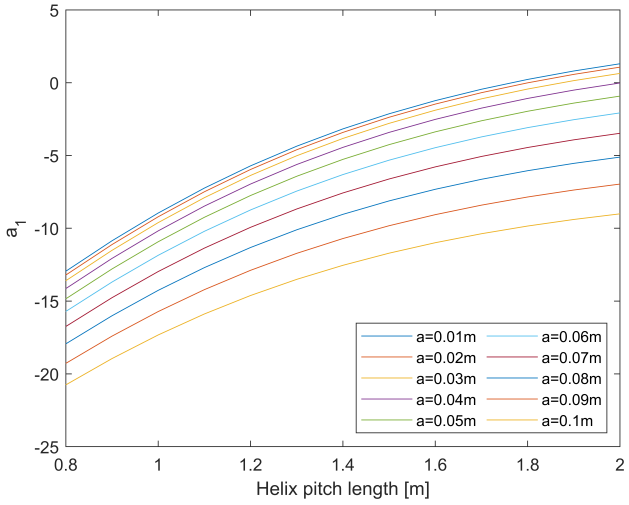

Figure 5.12: The parameter a_1 as a function of p

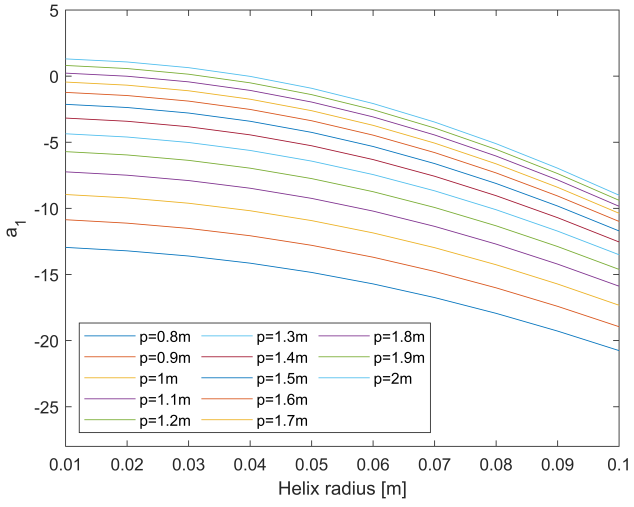

Figure 5.13: The parameter a_1 as a function of a

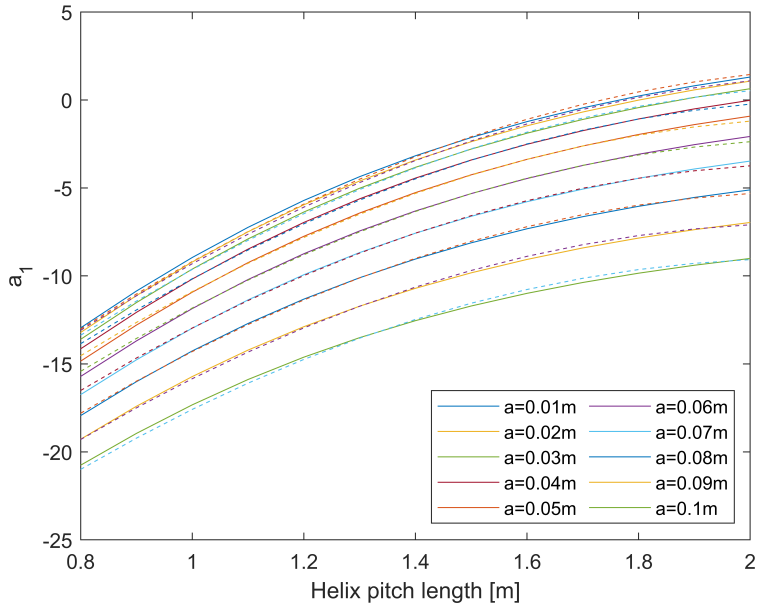

Figure 5.14: The parameter a_1 and its approximation as a function of p

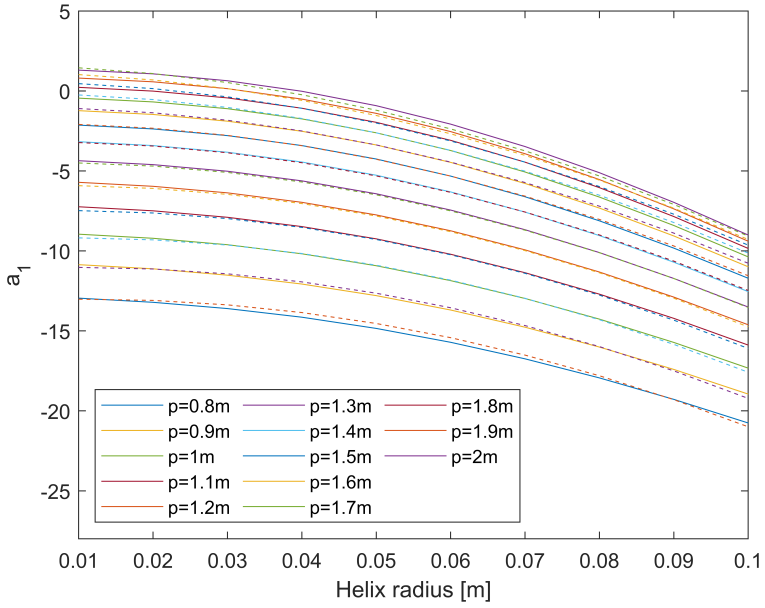

Figure 5.15: The parameter a_1 and its approximation as a function of a

5.2.3 The parameter a_2

Also the parameter a_2 could be considered as a two-degree function of both the helix radius a and the pitch p

$$a_2 \approx 0.1719 - 0.2132p - 0.1793a + 0.05702p^2 - 0.07299pa + 9.837a^2 \quad (5.13)$$

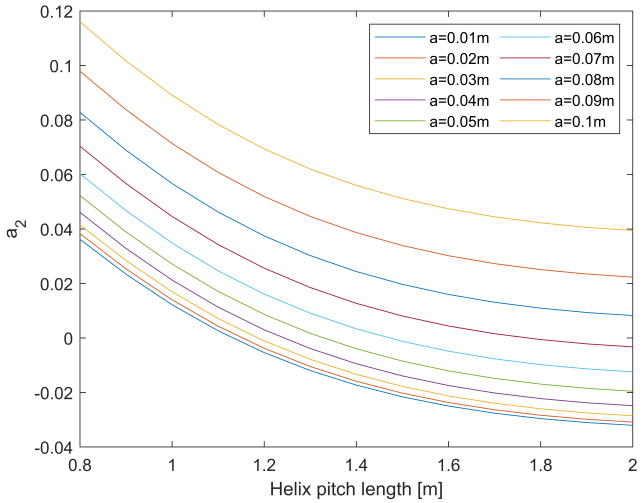

Figure 5.16: The parameter a_2 as a function of p

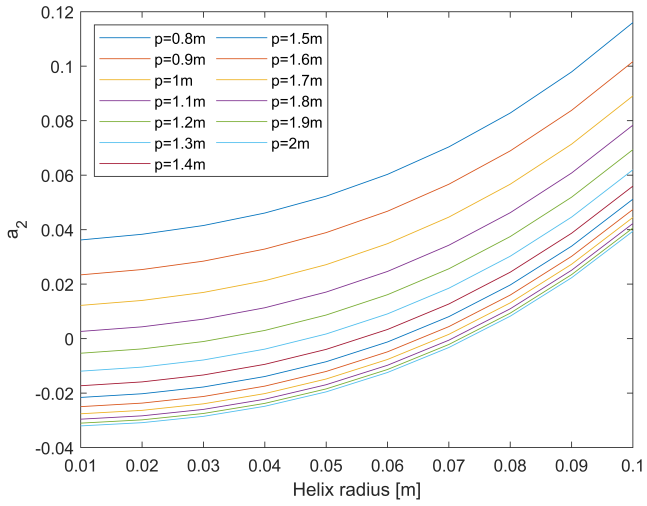

Figure 5.17: The parameter a_2 as a function of a

It can be noticed that the (5.13) does not approximate very properly the exact values of a_2, indeed higher polynomial degree have to be considered to reduce the errors, but it is shown later that the final results are still good enough, so it is not necessary to further complicate the formulation.

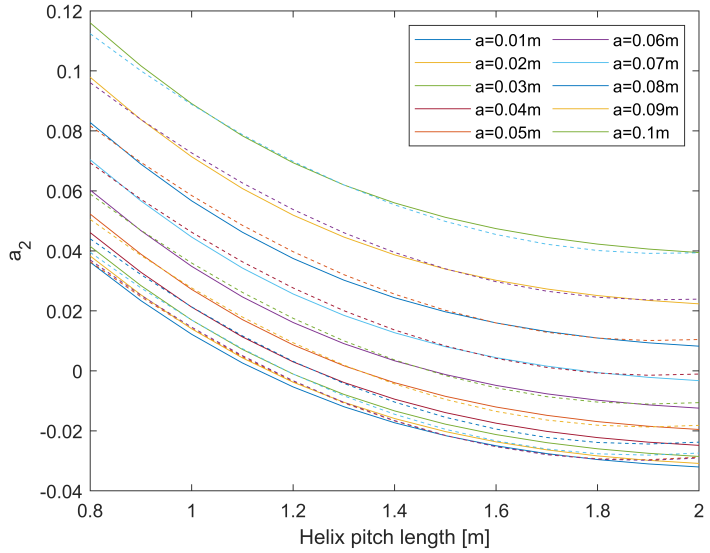

Figure 5.18: The parameter a_2 and its approximation as a function of p

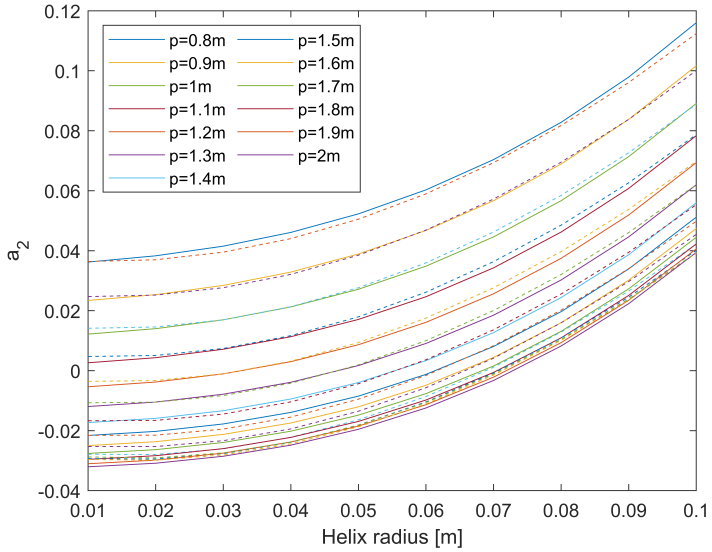

Figure 5.19: The parameter a_2 and its approximation as a function of a

5.2.4 The parameter a_4

As the previous parameters, a_4 has a quadratic dependence on both a and p

$$a_4 \approx 35.14 - 32.82p - 43.74a + 7.188p^2 + 22.44pa + 1147a^2 \tag{5.14}$$

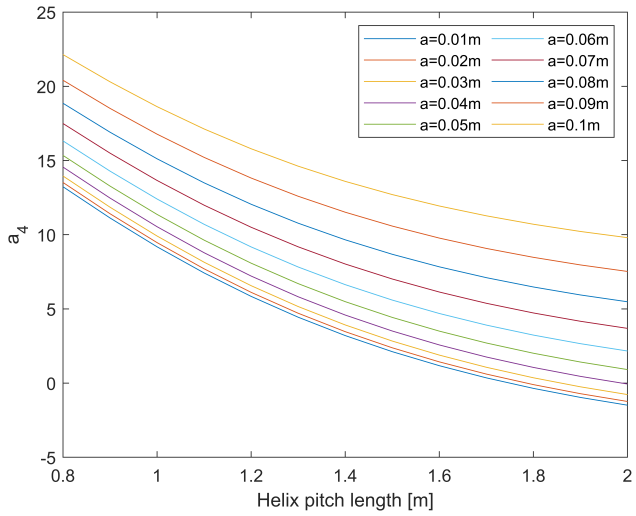

Figure 5.20: The parameter a_4 as a function of p

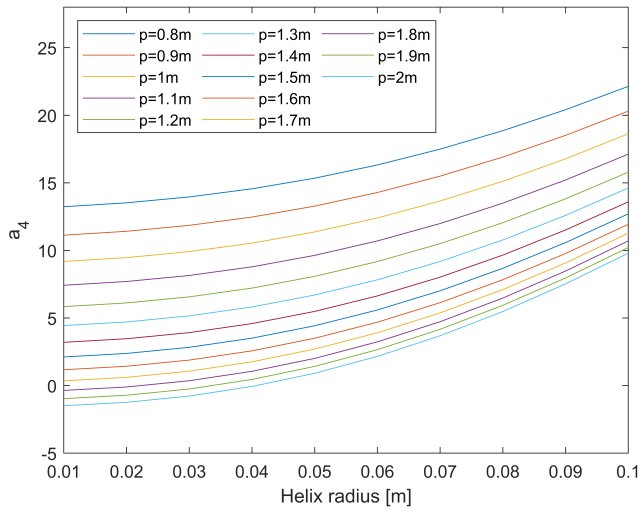

Figure 5.21: The parameter a_4 as a function of a

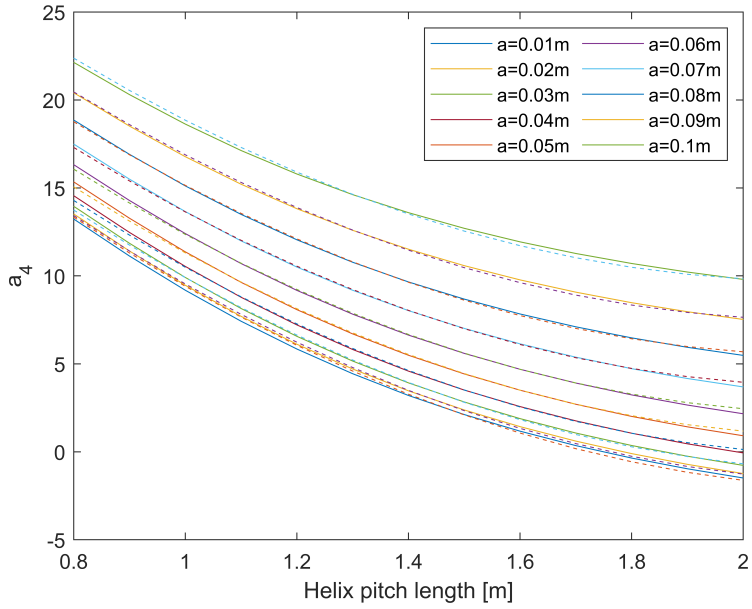

Figure 5.22: The parameter a_4 and its approximation as a function of p

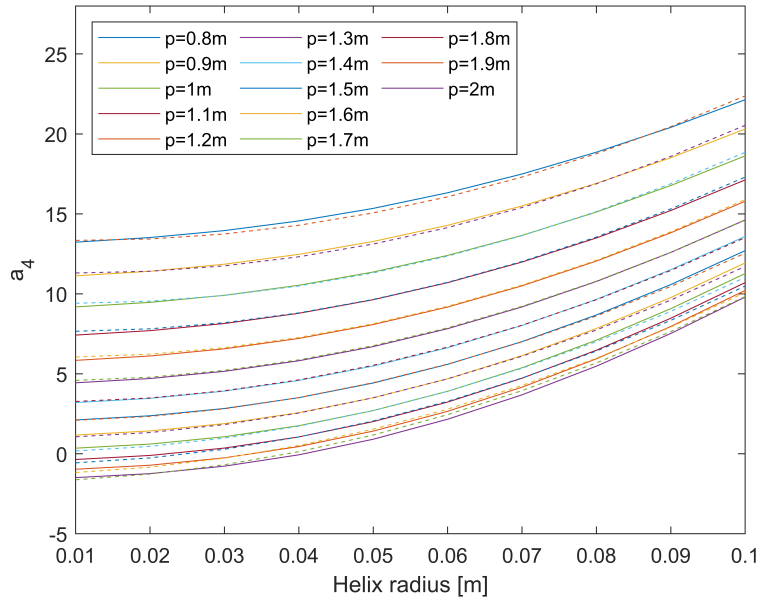

Figure 5.23: The parameter a_4 and its approximation as a function of a

5.2.5 The parameter a_5

The parameter a_5 has a cubical dependence on p and a quadratic on a

$$a_5 \approx 0.05075 + 0.004659p - 0.03289a - 0.007306p^2 - 0.01004pa + \\ + 1.635a^2 + 0.00195p^3 + 0.00222p^2a - 0.02515pa^2 \tag{5.15}$$

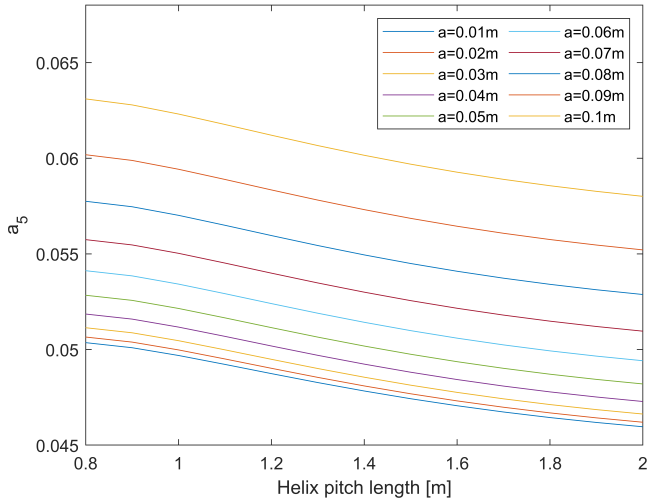

Figure 5.24: The parameter a_5 as a function of p

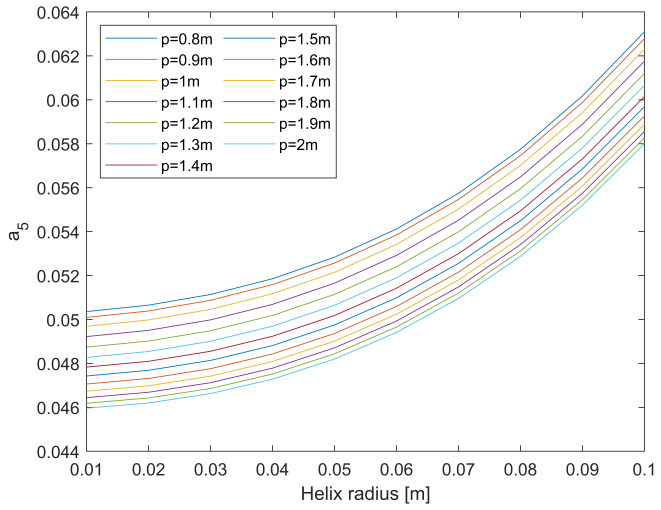

Figure 5.25: The parameter a_5 as a function of a

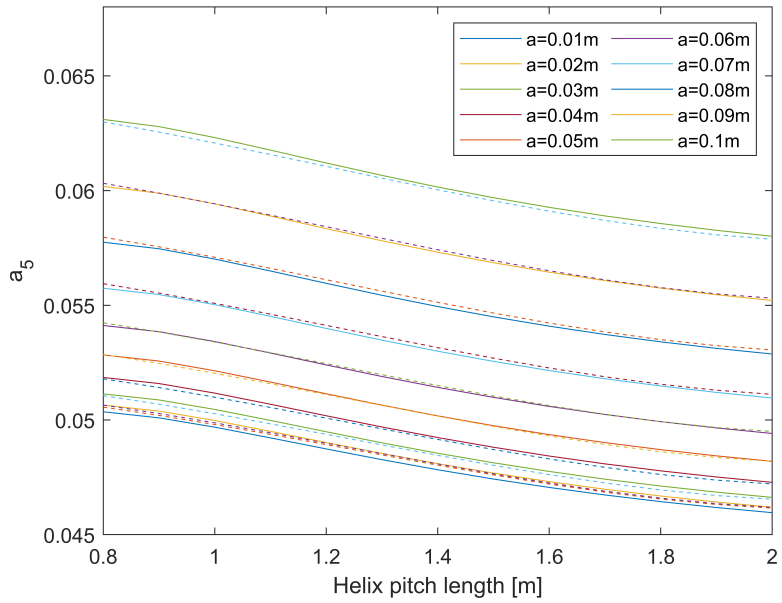

Figure 5.26: The parameter a_5 and its approximation as a function of p

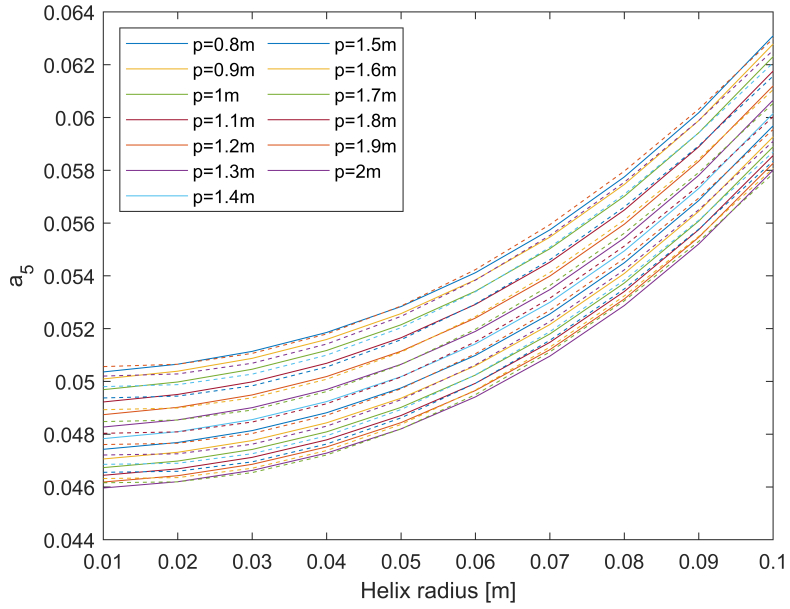

Figure 5.27: The parameter a_5 and its approximation as a function of a

The results obtained by substituting the approximate polynomial equations (5.11÷5.15) in the equation of the field (5.9) are not bad: generally the results coincides or even overestimate the field; the errors are higher for the increase of r; the highest error equal to 8.1067% is obtained with $a = 0.06m$, $p = 0.8m$ at $r = 2m$, but in this case the field is overestimated, so it is advantageous; there are cases where fields are underestimated, the highest one present an error equal to -6.1140% with $a = 0.1m$, $p = 1m$ at $r = 2m$, but the field present a value equal to $1.4495\mu T$, so the uncertainty is on the second decimal place and could be neglected. In conclusion, the results are good, although much more complex than Landini's one, however the field can be calculated by means of the lookup tables with a simply calculator.

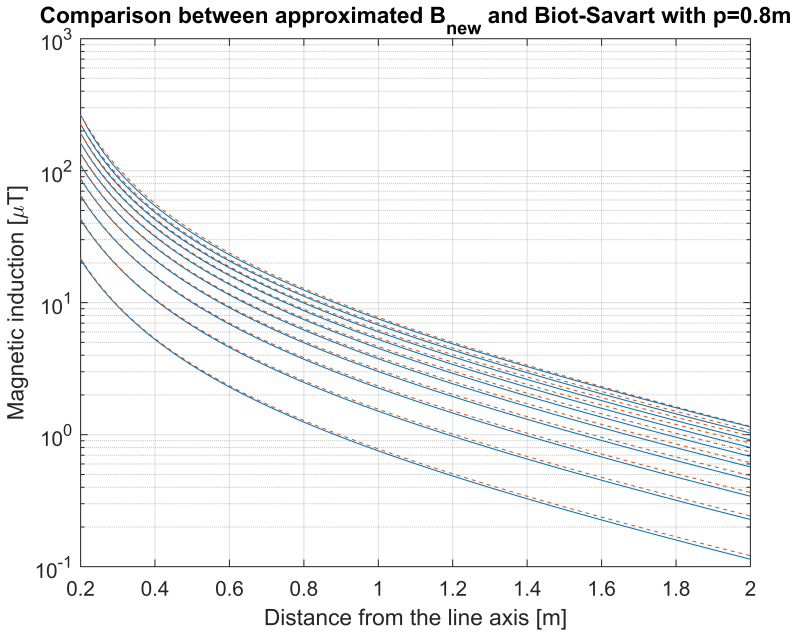

Figure 5.28: Approximated B_{new} compared to Biot-Savart

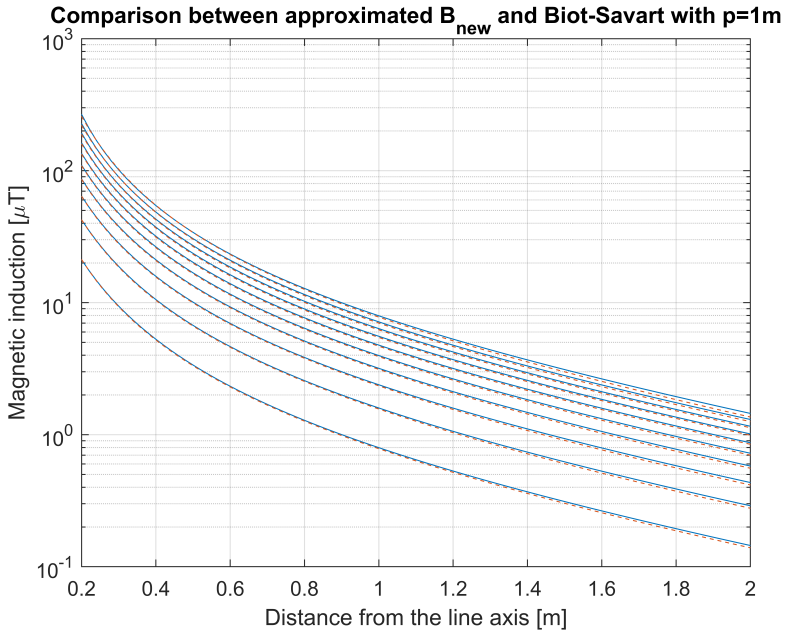

Figure 5.29: Approximated B_{new} compared to Biot-Savart

5.3 Matlab codes

The Curve Fitter codes are automatically generated by Matlab, then they will not be shown. Instead the codes used to implement the Landini's approximated parametric equation is really simply

Listing 5.1: Landini's parametric equation

```
%% Data

I=200; % rms value [A]
a=0.01:0.01:0.1; % helix radius [m]
p=0.8; % helix pitch [m]
r=[0.2:0.02:2 2:0.5:5]; % radial distances [m]

N=2;    phi=0;
[Besatto]=Bessel3F(a,p,r,N,phi,I);

%% Landini
% ln(B) = ln(2.4*pi^2*a/p^2) + ln(I) + [ao+a1*r+a2/(r^
    a3)]
%       = ln(G) + ln(I) + [ao+a1*r+a2/(r^a3)]
```

```
a0lan=zeros(length(a),length(p));
a1lan=zeros(length(a),length(p));
a3lan=zeros(length(a),length(p));
Blan2=zeros(length(a),length(r),length(p));

for ia=1:length(a)
a0lan(ia,:)=(12.8712*a(ia)^2+0.2107*a(ia)-0.1383)*p
   .^2+(-48.4318*a(ia)^2-0.6919*a(ia)+0.9094)*p
   +49.6932*a(ia)^2+0.5724*a(ia)-1.3991;
a1lan(ia,:)=2.1018*p.^3-11.6186*p.^2+...
            23.2879*p-20.4446;
a3lan(ia,:)=0.2739*a(ia)*p+0.2430*p+...
            0.1036*a(ia)+1.4444;
    for ip=1:length(p)
        Blan2(ia,:,ip)=log(2.4*pi^2*a(ia)/p(ip)^2)+...
                log(I)+a0lan(ia,ip)+a1lan(ia,ip)*r+...
                0.1./(r.^a3lan(ia,ip));
    end
end

dBlan2=exp(Blan2)-Besatto;
dBrellan2=(Besatto-exp(Blan2))./Besatto*100;
```

5.4 Appendices

Table 5.1: Parameter a_0

p $[m]$	**a** $[m]$									
	0,01	0,02	0,03	0,04	0,05	0,06	0,07	0,08	0,09	0,1
0,8	-44,90	-44,93	-44,98	-45,05	-45,14	-45,26	-45,41	-45,59	-45,82	-46,09
0,9	-44,61	-44,64	-44,68	-44,75	-44,84	-44,96	-45,10	-45,29	-45,51	-45,78
1	-44,33	-44,35	-44,40	-44,46	-44,55	-44,67	-44,81	-44,99	-45,21	-45,48
1,1	-44,06	-44,09	-44,13	-44,20	-44,28	-44,40	-44,54	-44,72	-44,94	-45,20
1,2	-43,82	-43,84	-43,89	-43,95	-44,03	-44,15	-44,29	-44,46	-44,68	-44,94
1,3	-43,59	-43,61	-43,66	-43,72	-43,80	-43,91	-44,05	-44,23	-44,44	-44,70
1,4	-43,38	-43,40	-43,44	-43,51	-43,59	-43,70	-43,84	-44,01	-44,22	-44,48
1,5	-43,19	-43,21	-43,25	-43,31	-43,39	-43,50	-43,64	-43,81	-44,02	-44,28
1,6	-43,01	-43,03	-43,07	-43,13	-43,21	-43,32	-43,46	-43,63	-43,84	-44,09
1,7	-42,84	-42,87	-42,91	-42,96	-43,04	-43,15	-43,29	-43,46	-43,67	-43,92
1,8	-42,69	-42,71	-42,75	-42,81	-42,89	-43,00	-43,13	-43,30	-43,51	-43,76
1,9	-42,55	-42,57	-42,61	-42,67	-42,75	-42,85	-42,99	-43,16	-43,36	-43,61
2	-42,42	-42,44	-42,48	-42,53	-42,61	-42,72	-42,85	-43,02	-43,23	-43,48

Table 5.2: Parameter a_1

p	**a** $[m]$									
$[m]$	0,01	0,02	0,03	0,04	0,05	0,06	0,07	0,08	0,09	0,1
0,8	-12,95	-13,21	-13,60	-14,14	-14,85	-15,71	-16,75	-17,94	-19,28	-20,76
0,9	-10,86	-11,12	-11,52	-12,07	-12,79	-13,69	-14,77	-16,01	-17,41	-18,95
1	-8,955	-9,211	-9,613	-10,18	-10,93	-11,86	-12,97	-14,26	-15,72	-17,33
1,1	-7,240	-7,493	-7,899	-8,478	-9,246	-10,21	-11,36	-12,70	-14,22	-15,89
1,2	-5,712	-5,962	-6,370	-6,962	-7,750	-8,741	-9,934	-11,32	-12,89	-14,62
1,3	-4,361	-4,607	-5,019	-5,621	-6,428	-7,447	-8,675	-10,10	-11,72	-13,51
1,4	-3,173	-3,416	-3,831	-4,443	-5,268	-6,312	-7,573	-9,043	-10,71	-12,54
1,5	-2,135	-2,375	-2,793	-3,414	-4,255	-5,322	-6,614	-8,120	-9,825	-11,71
1,6	-1,232	-1,469	-1,890	-2,520	-3,376	-4,465	-5,783	-7,322	-9,065	-10,99
1,7	-0,450	-0,686	-1,109	-1,747	-2,616	-3,724	-5,067	-6,635	-8,411	-10,37
1,8	0,225	-0,010	-0,436	-1,081	-1,962	-3,087	-4,451	-6,045	-7,851	-9,846
1,9	0.805	0.572	0.143	-0.509	-1.401	-2.541	-3.925	-5.541	-7.372	-9.394
2	1.301	1.069	0.638	-0.020	-0.921	-2.074	-3.475	-5.111	-6.964	-9.008

Table 5.3: Parameter a_2: it have to be multiplied by 10^{-3} for the application

p	**a** $[m]$									
$[m]$	0,01	0,02	0,03	0,04	0,05	0,06	0,07	0,08	0,09	0,1
0,8	36,22	38,30	41,52	46,10	52,28	60,29	70,38	82,80	97,89	116,02
0,9	23,41	25,36	28,44	32,88	38,91	46,76	56,67	68,91	83,78	101,69
1	12,20	14,01	16,96	21,26	27,15	34,85	44,60	56,68	71,38	89,10
1,1	2,638	4,328	7,147	11,33	17,09	24,66	34,28	46,22	60,78	78,35
1,2	-5,359	-3,779	-1,068	3,003	8,657	16,12	25,63	37,46	51,91	69,37
1,3	-11,95	-10,46	-7,841	-3,861	1,704	9,079	18,50	30,24	44,60	61,98
1,4	-17,30	-15,89	-13,35	-9,441	-3,949	3,355	12,71	24,38	38,68	55,98
1,5	-21,59	-20,24	-17,76	-13,91	-8,479	-1,232	8,068	19,68	33,93	51,19
1,6	-24,97	-23,67	-21,24	-17,44	-12,05	-4,850	4,407	15,98	30,19	47,41
1,7	-27,59	-26,33	-23,94	-20,18	-14,82	-7,654	1,571	13,12	27,29	44,48
1,8	-29,57	-28,35	-25,98	-22,25	-16,92	-9,778	-0,576	10,95	25,10	42,26
1,9	-31,02	-29,82	-27,48	-23,77	-18,46	-11,34	-2,154	9,351	23,48	40,61
2	-32,04	-30,86	-28,53	-24,84	-19,54	-12,43	-3,263	8,227	22,34	39,43

Table 5.4: Parameter a_4

p	**a** $[m]$									
$[m]$	0,01	0,02	0,03	0,04	0,05	0,06	0,07	0,08	0,09	0,1
0,8	13,23	13,52	13,96	14,56	15,34	16,32	17,49	18,86	20,41	22,14
0,9	11,13	11,41	11,85	12,47	13,28	14,28	15,50	16,91	18,51	20,30
1	9,185	9,467	9,911	10,54	11,37	12,41	13,66	15,11	16,78	18,63
1,1	7,423	7,700	8,146	8,785	9,634	10,70	11,99	13,50	15,21	17,13
1,2	5,843	6,116	6,564	7,213	8,080	9,176	10,50	12,05	13,82	15,79
1,3	4,439	4,707	5,158	5,817	6,702	7,823	9,183	10,77	12,59	14,62
1,4	3,202	3,466	3,918	4,586	5,488	6,634	8,025	9,655	11,52	13,59
1,5	2,117	2,378	2,833	3,509	4,426	5,594	7,014	8,680	10,58	12,70
1,6	1,172	1,430	1,887	2,571	3,502	4,690	6,136	7,834	9,771	11,93
1,7	0,352	0,608	1,067	1,758	2,702	3,908	5,378	7,104	9,074	11,27
1,8	-0,356	-0,103	0,358	1,056	2,012	3,235	4,725	6,477	8,475	10,70
1,9	-0,966	-0,714	-0,251	0,453	1,419	2,656	4,166	5,939	7,962	10,22
2	-1,489	-1,238	-0,773	-0,064	0,911	2,162	3,687	5,480	7,524	9,800

Table 5.5: Parameter a_5: it have to be multiplied by 10^{-3} for the application

p	**a** $[m]$									
$[m]$	0,01	0,02	0,03	0,04	0,05	0,06	0,07	0,08	0,09	0,1
0,8	50,36	50,65	51,14	51,85	52,84	54,12	55,74	57,75	60,18	63,10
0,9	50,09	50,39	50,87	51,59	52,57	53,85	55,47	57,46	59,88	62,79
1	49,69	49,98	50,46	51,17	52,15	53,42	55,03	57,01	59,42	62,31
1,1	49,22	49,51	49,98	50,69	51,65	52,92	54,52	56,49	58,89	61,76
1,2	48,74	49,02	49,49	50,19	51,14	52,40	53,99	55,96	58,34	61,20
1,3	48,27	48,54	49,01	49,70	50,65	51,90	53,48	55,44	57,81	60,66
1,4	47,83	48,10	48,55	49,24	50,18	51,42	53,00	54,95	57,31	60,15
1,5	47,43	47,69	48,14	48,81	49,75	50,99	52,56	54,50	56,86	59,69
1,6	47,06	47,31	47,76	48,43	49,36	50,59	52,16	54,09	56,44	59,27
1,7	46,73	46,98	47,42	48,09	49,02	50,24	51,80	53,73	56,08	58,89
1,8	46,44	46,69	47,12	47,79	48,71	49,93	51,48	53,41	55,75	58,56
1,9	46,19	46,43	46,86	47,52	48,44	49,66	51,20	53,12	55,46	58,27
2	45,96	46,20	46,63	47,28	48,20	49,41	50,96	52,88	55,21	58,01

Chapter 6

Conclusions

In the thesis all the methods for the calculation of the magnetic field generated by twisted three-phase cables were implemented in order to compare them and to looking for the more simpler and the fast between them.

First of all it is implemented on Matlab the classic formulation used for the magnetic field calculations, that are the Biot savart Law in both the two-dimensional and the three-dimensional formulation, the bidimensional one is used for the verification of the three-dimensional method's correctness on the case of a single-circuit underground power line in trefoil formation, once the validity of the Biot-Savart 3D codes is confirmed, it is applied in the field calculation of the twisted tripolar cable, its results are used as reference for all other methods.

Secondly, Hagel series formulation (which include the modified Bessel functions and its first derivatives) in cylindrical coordinates is implemented, it turns out that its results may be good for cases with lower helix radius a and greater helix pitch p, but generally errors are high, since it goes to zero very quickly, thus for the buffer zone estimation some cautionary distances have to be added.

Since the Bessel functions are complex, alternative methods are derived from Hagel, in particular Pettersson proposes the reduction of the series at the first term with further approximations considering $a << p$ and $r >> p$, but these formulations provide results with really high errors in the immediate vicinity of the cable, anyway they give still valid results for sufficiently far distances in comparison respect to the complete series formulation.

Finally, it is analyzed the parametric method proposed by Landini based on the approximation to the first two terms of the series, the results he obtained are very good in comparison to the series, but this solution still shows not negligible errors compared to the values of Biot-Savart.

Then it is decided to apply Landini's method directly on the results of Biot-Savart obtaining the following parametric formulation

$$ln(B_{new}) = ln\left(2.4\pi^2 \frac{a}{p^2}\right) + ln(I) + a_0 + a_1 r + a_2 r^2 + \frac{a_3 + a_4 r}{r^{a_5}} \qquad (6.1)$$

this equation can provide estimates of the magnetic field almost coincident with Biot-savart Law in the range of distances from 0.2m to 5m. The parameters $a_{0 \div 5}$ (except a_3 which is fixed to 40) can be used quickly by means of lookup tables as a function of a and p; the relationship between the parameters with a and p can be expressed approximately with polynomials. The overall the formulation is longer than the one proposed by Landini, but it provides better results.

Bibliography

[1] AIRC. *È vero che i campi elettromagnetici aumentano la probabilità che insorga il cancro?* URL: https://www.airc.it/cancro/informazioni-tumori/corretta-informazione/vero-campi-elettromagnetici-aumentano-la-probabilita-insorgenza-del-cancro#:~:text=Il%20principale%20effetto%20biologico%20della,dall'esposizione%20a%20lungo%20termine..

[2] ARPAV. *CONTROLLO DELL'INQUINAMENTO ELETTROMAGNETICO SUL TERRITORIO DELLA REGIONE VENETO 2022*. Tech. rep. 2022.

[3] CEI. *Guida per la determinazione delle fasce di rispetto per gli elettrodotti secondo le disposizioni del DPCM 8 luglio 2003 (Art. 6) Parte 1: Linee elettriche aeree e in cavo*. Tech. rep. 2006.

[4] G. MAZZANTI E. KANDIA M. LANDINI. "Calcolo del campo magnetico generato da cavi elicordati per la distribuzione dell'energia elettrica". In: (2009).

[5] Wojciech MACHCZYŃSKI Krzysztof BUDNIK. "ANALYTICAL MAGNETIC FIELD CALCULATION OF HELICAL CURRENT CONDUCTORS". In: (2010).

[6] R. Unbehauen R. Hagel L. Gong. "On the Magnetic Field of an Infinitely Long Helical Line Current". In: *IEEE TRANSACTIONS ON MAGNETICS, VOL. 30, NO. I , JANUARY 1994* (1994).